Wear characteristics, reduction techniques and its application in automotive parts – A review

Luke O. Ajuka[1], Omolayo M. Ikumapayi[2*], Esther T. Akinlabi[3]

[1]Department of Automotive Engineering, University of Ibadan, Oyo State, Nigeria
[2]Department of Mechanical Engineering Science, University of Johannesburg, South Africa
[3]Department of Mechanical and Construction Engineering, Northumbria University, Newcastle, United Kingdom

[*]Correspondence E-mail: ikumapayi.omolayo@gmail.com

ABSTRACT

Wear phenomenon impact the operating efficiency and service life of engineering materials due to the influence of surface interaction at different working conditions. Successive tribological studies on wear-resistant materials in the last decade is estimated at approximately 40% of friction and wear, including laboratory tests. Most locally improvised wear testers in accordance with American Society for Testing and Materials (ASTM) and European (EN) standards, though, achieves 95-97% parametric accuracies with reduced cost, they hardly harmonize degradation and Archard's coefficients for all possible wear factors, providing little data for simulation of mechanical and chemical wears which are responsible for non-uniform aggregation of wear patterns in practice. Complexities of intermeshing factors which combine to influence the effectiveness of developed test devices span over loads, speeds, temperature, pressures and ambience for various applications. This study highlights the techniques of wear characterization, test standards and wear reduction with emphasis on surface texturing for improved eta/beta phase re-arrangements at low working temperatures in the enhancement of grain contraction during high bias-voltage cathodic substrate multi-phase coating, phosphating during pretreatments using peening techniques, residual stress reduction during cryogenic heat treatments as well as the impact of suitable architectural matrix composite strengthening, microstructures and material reinforcements as suitable factors to influence improved tribological behaviors in materials. Optimal additive manufacturing (AM-fabricating) techniques with pretreatments, thermal cycling and tempering can engineer enhanced anti-tribocorrrosion in Automotive components.

Keywords: ASTM and EN Standards, Materials, Reduction techniques, Wear, Automotive components.

PUBLIC INTEREST STATEMENT

This research aimed at providing a basis and state-of-the-art review on wear characteristics, test, reduction techniques and application in automotive parts. It

highlights existing test standards (ASTM and EN)) from which other developed wear test devices accuracies are measured and point at the limitations, for example, high sensitivity level in varying load, speeds, temperature, pressures and ambience which should be factored in the improvised test devices, to scale-up their standards for various applications. It highlights the importance of surface engineering through surface coating, texturing or layering, hardening and architecture, as well as composition strengthening of microstructure and reinforcements as a means to promote anti-tribocorrosion of materials. It then highlights the influence of pretreatments like Laser shock peening which can cause considerable reduction in electrochemical corrosion by approximately 80%, and cryogenic heat treatment (especially deep cryogenic heat treatment) as a means to enhance mechanical properties of materials due to reduction residual stress and coefficient of friction, improve of anti-wear, hardness, toughness and fatigue resistance in automotive parts. This paper provides unalloyed and intrinsic information for development of reliable and reproduceable local wear test devices and automotive parts with high anti-wear properties in extreme environment. The reliable data so provided can lead to robust analysis from big data provided through this wear testing systems.

ABOUT THE AUTHORS

Luke O. Ajuka is a Lecturer in the department of automotive Engineering, University of Ibadan, Nigeria. He holds B.Eng., M.Sc. and Ph.D. degrees in Mechanical Engineering. He has published papers on refrigeration and automotive systems. His research interests include HVAC systems, energy, characterizations, applied nanotechnology, automotive fuel and systems.

Temitayo S. Ogedengbe, PhD is a Lecturer in the department of Mechanical Engineering, Nile University, Abuja, Nigeria. He earned his Ph.D degree at the Department of Mechanical Engineering, University of Ilorin, Kwara State, Nigeria. His research interests include additive manufacturing, machining, material processing, processing using agro-wastes powders, surface modifications, characterizations, welding and nanotechnology.

Timothy Adeyi holds B.Eng. and M.Sc. degrees in Mechanical Engineering and lectures at the Department of Mechanical Engineering, Lead City University, Ibadan, Nigeria. He is currently pursuing his PhD at the University of Ibadan, Nigeria.

Omolayo M. Ikumapayi, PhD is a Senior Lecturer in the department of Mechanical and Mechatronics Engineering, Afe Babalola University, Ado Ekiti, Nigeria. He earned his Ph.D degree at the Department of Mechanical Engineering Science, University of Johannesburg South Africa. His research interests include additive manufacturing, simulation, processing using agro-wastes powders, surface

modifications, characterizations, tribocorrossion, Friction stir processing/welding, automation, mechatronics, and nanotechnology.

Esther T. Akinlabi is currently a Full Professor in the Department of Mechanical and Construction Engineering and Deputy Faculty Pro Vice-Chancellor, Faculty of Engineering and Built Environment (FEBE), Northumbria University, United Kingdom. She has authored several peer-reviewed scholarly Journals, Books, and Book Chapters. Her areas of interests are in Energy, Friction Stir Welding/Processing, additive manufacturing, laser manufacturing, AutoCAD, Research Design etc.

List of Abbreviations

AM - Additive manufacturing
ASTM-American Society for Testing and Materials
EN – European
EDXS – Energy Dispersive X-ray Spectroscopy
PDC–Polymer Derived Ceramic
XPS – X-ray photoelectron microscopy
TEM – Transmission Electron Microscopy
CR-AFM- Contact Resonance AFM
BTR- Blind Tip Reconstruction
FCC-Face Cubic Centered
SPD-Severe Plastic Deformation
AHSS-Advanced High-Strength Steel
$B^{1-x}C^{x}$- Amorphous Boron Carbide
MoS_2-Molybdenum disulphide
CrFeCoNiMo- Alloy
CNTs-Carbon Nanotubes
DLC-Diamond-like Carbon
Ti_3C_2Tx-Titanium Carbide
Si_3N_4-Silicon Nitride
WC-Co-Tungsten Carbide-Cobalt
TiC- Titanium Carbide
TiN-Titanium Nitride
Zr-Zirconium
HNO_3-Nitric Acid
SEM/LM–Scanning Electron Microscopy/Light Microscopy; **CoF**-Coefficient of Friction
HV-Vickers Hardness
ICE-Internal Combustion Engine

1. Introduction

Wear on material surfaces is a common phenomenon that involves slow erosion or displacement. This is due to the action of a solid surface rubbing, sliding, meshing, or grinding on another surface, contacts [Rosenkranz et al., 2019], e.g., the valves responsible for internal combustion engine cylinder opening to allow-in fuel-air mix during intake stroke, gas sealing in the cylinder, and combustible gas removal during exhaust stroke experience a service life of valve train dynamic stress due to thermal load caused by valve seat's deformation, this contact gradually becomes uneven, resulting in a progressive partial contact prior to failure [Rosenkranz et al., 2021]. Wear is seen in automobile components such as tires [Gachot et al., 2017], internal combustion engine (ICE) cylinder [Koszela et al., 2018], journal and thrust bearing [Rosenkranz et al., 2019], piston rings [Profito et al., 2017; Zimmer et al., 2021], etc. Wear is a system response, not a property. It

leads to the replacement of engineering components and assemblies as a result of lower operational efficiency due to power losses, oil consumption, and component replacement rates [Calderon, 2022], for example, in biomedical applications, anti-wear is essential to prevent joint replacements. As a result, wear-related imperfections on surfaces become even more significant [Wang et al., 2020]. Even on the hardest material, diamond, wear extent is a consequence of prevalent conditions at that operating state, including valve trains, bore rings, and grooves [Hareesha and Jeevan, 2014]. Meanwhile, it has been reported that a formulated combination of engineering design and guidelines for effective selection of materials with bias for various stress-strain compositions, rates, and microstructures should be investigated [Psyllaki, 2019]. To address the limitation of material service life caused by the rate of wear, various wear investigations conducted on surface have ranged from material removal, film transfer, inelastic fractures, plastic distortion, and tribology. This implies that laboratory experiments are used to imitate real-world settings, and that the wear processes seen in lab studies are the same as those seen in practice. Furthermore, rapid needle tip wear in an atomic force microscope (AFM), failure, and tissue reactions (osteolysis and sepsis) caused by wear debris in orthopaedical joint implants contributes to the ever-challenging wear issues that necessitate ongoing wear resistance research at both the nanoscale and macroscale [Patrick et al., 2016; Parande et al., 2016]. In automotive systems, contacts are inevitable, steel and aluminum alloys are the workhorse materials mostly employed, owing to their good mechanical properties and relatively low cost [Gullino et al., 2019], meanwhile, the knowledge of anti-tribocorrosion in the ever-growing industries will aid the optimized manufacture of high multifunctional and service-life components with structural integrations to perform in extreme environmental conditions. Hence, the goal of this work is to highlight recent advancements in wear characterization, wear mitigation, and consequences on tribo-components including automotive parts.

In this study, the first section presents an overview of this review and highlights the mechanisms of wear, wear test selection and characterization techniques. The second section highlights the techniques of wear reduction and composition strengthening, while the third section briefly describes the wear reduction employed in Automotive Parts before conclusion.

1.1 Mechanisms of Wear

Wear has two major categories; wear dominance by mechanical characteristics of materials and one dominated by chemical characteristics of materials (Table 1). Seven mechanical wear mechanisms form exists, however, only three surfaces-surface interaction can lead to them [ASTM, 1995]: sliding (a surface which slides over another over long distances), fretting (minute distance oscillation of one surface relative to the other) and erosion (external source impingement of solid particle on a single surface). In practice, dry sliding wear mechanisms depends on some variables and includes: surface finish, geometry, orientation, sliding speed, relative hardness (of one surface relative to the other or abrasive particles between the surfaces), and material microstructure. These variables reveal that wear rate is independent of pure material property and its occurrence is non-uniform [Prabhu et *al.*, 2014].

Table 1. Wear Classifications and Mechanisms **[**Bayer, 2002**]**

S/N	Classification	Wear Mechanisms	Wear coefficient K (range)
1	Wear dominance via by material mechanical characteristics.	• Asperity deformation and removal • Plowing Wear caused by plowing • Delamination wear • Adhesive wear • Abrasive wear • Fretting wear • Wear impinged by solid particle	10^{-4} 10^{-4} 10^{-4} 10^{-4} 10^{-2} to 10^{-1} 10^{-6} to 10^{-4}
2	Wear dominance via by material chemical characteristics.	• Solution wear • Oxidation wear • Diffusive wear • Wear by surface layer melting • Adhesive wear by high temperatures	

It has been reported that a single method of wear testing is insufficient [ASTM 1995]. This has resulted in the development of wear testing machines by modifying existing standard machines, as briefly highlighted;

Reniel et al. (2014) developed an abrasive wear testing machine based on the ASTM G65 standard. They emphasized the device's significance in tribology and stated that attrition loss could be quantified by evaluating mass or dimension disparities in an erosive wear environment. They classified the test methodologies into five alphabetical groups based on the loads and slide distances A, B, C, D, and E. They find that the dry sand-rubber wheel device conformed with ASTM G 65 within the stipulated work requirements at a lower cost. Nassar and Nassar (2011) developed a pin-in-disc wear tester for metallurgical research utilizing locally sourced materials. They revealed that as load decreases from 29.4N to 49 N and time decreases from 240 to 120 seconds, the rate of wear decreases. They statistically compared the tester to a foreign standard existing wear device under the same test settings and reported that it was 97 percent effective. Ogedengbe et al. (2018) developed and tested a wear device. They ran design calculations on brass and copper materials and compared the results to the main shaft, compression spring, belt, pulley, and electric motor. Performance after development was compared to that of existing wear testers. After conducting a reliability test, they concluded that the whirling observed on the shaft was as a result of the transmitted power from the shaft and that the wear rate was amplified with applied pressure over time on the locally made wear tester, but gradually.

1.2 Wear Test Selection

As the practical application approaches, defining the complicated collection of intermeshing parameters that combine to determine the unit's performance throughout a variety of loads, speeds, temperatures, pressures, and conditions becomes increasingly difficult. When determining a proper wear test measurement, consideration must be given to [Govind et al., 2015]:

• wanted characteristics of the sample material;

• state of material; bulk form, thick or thin coating;
• suitability of forces and stress limits for test;
• presence of abrasives so as to record abrasive size, form, and velocity;
• nature of components contacts, whether it is only rolling, impact, sliding, or erosion, or a combination of these, with test samples surface finish being similar to that of real components;
• importance of temperature and humidity as factors;
• similarity of test environment with actual working environment;
• expected start to end of test; and
• how comparable the test materials used is with real life machine part material.

Some of these engineering material wear test methods are given in Table 2.

Table 2: Some common test/characterization methods include (See Appendix for schematic of classical test system):

S/No	Test Method	Applicable Characteristics	Ref
1	Sliding wear Test:		
	• Uniaxial Motion, Pin-on-disc (Fig. 9 in Appendix I)	A linear displacement transducer is used to monitor wear displacement.	[ASTM G99-95a, 1997]
	• Reciprocating Test System (RTS), ASTM G133 (Fig. 10 in Appendix I)	Used in interactions that involve both sinusoidal and linear motion (linear servo system).	[ASTM G133-95, 1997]
	• Fretting Test System (Fig. 11 in Appendix I)	Sliding wear with a motion amplitude of 250m	[Lin et *al.*, 2022]
	• Thrust Washer Test (Fig. 12 in Appendix I)	Contacts with a large conformal area that are used in conformal big area contacts	[Balic and Blanchet, 2005]
2	Vapor blast erosion test system, ASTM G 76 (Fig. 2 in Appendix I).	Utilizes a high-pressure gas stream and a nozzle geometry based on a power law relationship to erode material.	[ASTM G76-95, 1997].
3	Abrasive Test		
	• Loose Slurry Abrasive Testing (Fig. 3 in Appendix I)	To analyze sample wear volume, a three-body sample in micro-abrasion slurry is used.	[ASTM G65-94, 1997]
	• Two body steel wheel, ASTM B611 abrasion (Fig. 6 in Appendix I)	Through steel wheel slurry, this device is used to quantify mass loss and density.	[ASTM B611-85, 1995]

	• Rubber Wheel, Dry Abrasive, ASTM G65 (Fig. 4 in Appendix I) • Rubber Wheel, Wet Abrasive Slurry, ASTM G105 (Fig. 5 in Appendix I).	To calculate the volume of material lost, sand flow rotating rubber wheel was used. Used for rubber steel slurry mass loss and density measurements	[ASTM G65-89,1997] [ASTM G105-89, 1997].
4	Ball Cratering (Fig. 7 in Appendix I)	Used for thin hard coatings, polymeric films, and other monolithic materials	[Pinto et *al.*, 2021]
5	Slurry Jet Erosion Test device, ASTM A532-ClassIII A (Fig. 13 in Appendix I)	Used to measure erosive resistance in terms of abrasive particle size.	[Yousif and A.H. Ataiwi, 2018]

1.3 **Wear Characterization Techniques**

To express and quantify wear for purposeful reduction, sample tribological behavior must be assessed. Considerable number of characterization strategies are been deployed; it includes sample chemical analysis with energy-dispersive X-ray spectroscopy (EDXS/EDS) to analyze the composition of chosen sections. For wear mechanism or a post-test evaluation, a scanning electron microscope/light microscope (SEM/LM) are utilized [Pillar, 2009]. There is emphasis on the application of these techniques to measure volume loss of wear and nano-hardness in materials utilizing optical profilometry and nanoindentation combined with atomic force microscopy (AFM), highlighting the newness, accuracies, and progress in characterization techniques. Meanwhile, 3D surface roughness was measured using a 3D Talysurf equipment [Suresh et al., 2012]. They examined chemistry of surface with X-ray photoelectron spectroscopy (XPS). Volume loss relative to wear track was measured utilizing an optical profilometer/3D-profilometer. Lately, an atomic force microscope (AFM) was utilized to examine tribological processes of friction, surface roughness, scratching, and adhesion [Bhushan, 2008]. AFM with a gravity-sensing indentation could also be used to detect interesting mechanical parameters like modulus of elasticity and hardness. Table 3 lists some of these engineering material wear characterization methods:

Table 3: Some Characterization Techniques in Materials

S/No	Method	Applicable Characteristics	Ref
1	Nanoindentation	To assess material (100 nm features and > 5nm thickness of thin films) for comparative and quantitative hardness measurement, as well as scratching in order to evaluate wear resistance and thin film adhesion	[Zhou and Liu, 2022]
2	Scanning electron Microscopy (SEM).	Used to measure tip wear with a resolution of 50nm by analyzing wear images before and after the test.	[Tayebi et *al.*, 2010, Fletcher et *al.*, 2010]

3	Transmission electron microscopy (TEM).	To examine tip wear volume as small as 25 nm.	[Jacobs and Carpick, 2013]
4	Atomic Force Microscopy (AFM)	Utilized in calculating free resonance spectra for AFM tip wear relative position using three AFM cantilevers with built-in thermal calibration.	[Killgore et *al.*, 2011]
5	Blind tip reconstruction (BTR)	Used to define the aspect ratio of structures on the specimen through 3D information and in-situ measurement.	[Liu et *al.*, 2010; Liu et *al.*, 2010]
6	Pull-off force Monitoring (PFM)	Used in In-situ measurement of contact radius and adhesion work	[Tinnemann et *al.*, 2019]
7	Contact-resonance AFM (CR-AFM)	Used in In-situ measurement of the contact radius of an AFM-sample	[Tian et *al.*, 2008]

2. Wear Reduction Techniques in Engineering Materials

Wear is acknowledged to be caused by defective design, insufficient lubrication, inappropriate lubrication, terrible craftsmanship, rough finish on surface, insufficient clearance between surfaces, competition with dust/metal particles, effect of most air, water, and chemicals, effect of temperature, and improper tooling, with friction playing a key role. Reducing the coefficient of friction in machining operations offers numerous benefits, but it necessitates a change in tool design [Luka et al., 2019]. Hard coatings are subjected to shear, tensile, and compressive stresses, which can cause cracking and spalling failure, according to Abadias et al., (2018).
Porosity, insufficient substrate bonding, and, in some situations, limited thickness is some of the drawbacks of hard coatings [Jibran et al., 2021]. Surface wear reduction approaches include surface texturing, hardening, and structures.

Surface texturing (Efficient surface generation by topography-controlled reformation) includes:

i) increasing load-carrying capacity by enhancing hydrodynamic pressure over the surface texture, [Lin et *al.*, 2013]

ii) application of inlet-suction impact to introduce extra lubricants to the real contact area, [Li et *al.*, 2019]

iii) decrement in the true contact area, [Klimczak and Jonasson, 1994]

iv) lubricant storage through the reservoir impact, [Krupka, 2013]

v) debris trapping impact, which captures worn particles, [Boidi et *al.*, 2021]

Surface textures with micro- and nanoscale feature sizes have been used as safe identifying elements to enhance the solar cell efficiency, but they are still wearable, [Baharin et *al.*, 2016], laser interference patterning is effective in fabricating in-volume optical gratings on metallic, [Rosler et al., 2018; Bieda et *al.*, 2010], semiconductor, [Vega et *al.*, 2014], ceramic, [Fabris et *al.*, 2019] and polymeric surfaces [Fukumura *al.*, 1994], demonstrating a good solution to this wear issue.

Surface hardening, in contrast, is a simple and direct way of increasing sample surface hardness through heat treatment or mechanical manipulation, resulting in increased wear resistance and fatigue resistance. Surface wear resistance can be derived from wear volume, V using Archard's law: V = KlF/H, where K represents wear coefficient, l represents sliding distance, F represents applied force, and H represents hardness. Traditional methods (carburizing, nitriding, and boriding) use component surface elemental diffusion in an elevated-temperature ambience to cause underlayer phase alteration inside the microstructures, resulting in improved hardness.
Recently, Xing et al. (2017) used diffusive plasma surface, duplex hardening, [Ooi, 2012] alloyed laser surface, [Chi et al., 2018] microwave heating, [Vasudev et al., 2019] friction stir processing, [Sharma et al., 2015]. Wear reduction, along with the simultaneous influence of wear mechanisms at various chain levels, results in pyramidal and heterogeneous wear natures. The multi-scale textured hierarchical design and heterogeneous patterning of surfaces influences wear reduction through improved tribological behavior, according to architecture. Table 4 summarizes related studies on wear reduction;

Table 4: Wear Reduction by Surface Engineering

Material	**Sample Characteristics**	**Observation/Remark**	**Ref**
Coatings			
Deposition of 2D graphene (2D LG) and 3D graphene foam (3D GF) by means of drop-casting process onto DLC/H-DLC film	Achieved a low wear rate (7.22×10^{-8} mm³ N^{-1} m^{-1}, 40.91% reduction) for DLC+3D GF film and a low COF (0.05, 82.69% reduction) H-DLC+2D LG film.	Effect of 2D LG and 3D GF controlled the humid sensitivities of DLC/H-DLC film tribological behavior during tribo-test at a load of 5 N in moist air	Gu et al., 2022
Diamond-like carbon on MoS_2 coatings	Tests for wear sliding to match the mechanical component rigidity.	Generated wear sliding with less-friction protective layers.	[Chen et *al.*, 2017; Lin et *al.*, 2008]
Graphene - MoS2 ensembles to reduce friction and wear in DLC-Steel contacts	Explored the combination of steel and diamond-like-carbon (DLC) in sliding contact	Friction and wear reduced by 16 and 29 times and is attributed to formation of amorphous carbon mixed graphene layers at the sliding interface	Mutyala et al., 2019
MoS_2 doped Ti, Cr, Zr, Ni, Ti-Si, or Sb_2O_3	To prevent MoS_2 crystal structure distortion and improve hardness	Enhanced wear resistance and improve hardness.	[Singh et *al.*, 2015; Simmonds et *al.*, 2000; Ye et *al.*, 2016; Zabinski et *al.*, 1995; Kong, et *al.*, 2010]

MoS_2 doped Au nanoparticles.	To improve shearing and load-supporting capabilities for MoS_2.	Resulted into superior tribological behavior	[Scharf et *al.*, 2010]
Ni-P nanocomposite coatings	To enhance composite hardness under t ambient conditions	Resulted in elevated hardness (250–1524 HV). 1700–2000 HV was produced by additionally heat treating from 200–300 °C for 30–40 weeks.	[Fuadi, 2014; Balaraju et *al.*, 2003]
Ni-based coatings doped with each of SiC & CNTs	Compared SiC and CNTs were compared for wear resistance.	Compared to SiC, CNTs had higher wear resistance.	[Balaraju et *al.*, 2003; Jiaqiang et *al.*, 2006]
DLC composite coatings doped WC/amorphous	Combined 1±3 nm and 5–10 nm of amorphous particles and nanocrystal grain size to make up biphasic structure.	For metallic surfaces, WC/DLC coatings demonstrated improved hardness, higher strength, and good corrosion and wear resistance.	[Voevodin et *al.*, 1999]
Fe-based amorphous coatings doped Zr substrate	Used laser heat treatment to boost coating hardness by 22%.	Wear resistance of Zr was increased by 800%, and amorphous coating wear was reduced by 96%.	[Sahasrabudhe & Bandyopadhyay, 2014]
Hydrogen-free DLC and hydrogenated DLC:H coatings.	Compared the hydrogen-free DLC and hydrogenated DLC:H coatings for anti-wear.	Due to delamination in the presence of hydrogen, DLC coatings shown superior anti-wear performance versus DLC:H coatings.	[Li & Bhushan, 1999a]
$Ti_3C_2T_x$ nanosheets doped with steel.	Wear reduction was examined in the $Ti_3C_2T_x$nanosheet modified steel surface at a pressure of 0.8 GPa.	Ti3C2Tx-nanosheets showed a 2.7-fold wear reduction. At low humidity and moderate contact stress, it demonstrated excellent anti-friction and wear capabilities.	[Malaki, M. & Varma et *al.*, 2020; Marian et *al.*, 2020]
Ti_3C_2/nanodiamonds (MXene) composite and	Examined the composite MXene coatings' resistance to	Due to the rolling ability of nanodiamonds within Ti3C2 inter/inner layers and the development of the tribofilm, composite	[Yin et *al.*, 2019]

polytetrafluoroethylene	polytetrafluoroethylene's sliding wear.	MXene coatings showed exceptionally good wear resistance.	
Wear tests on TMD MoS_2-16 at. % Ag film in atomic oxygen (AO) environment	Oxidization changed film morphology from dentrite-like surface for the non-irradiated film to the terrace-like one, and chrysanthemum-like one as the AO influence increased	Sputtered MoS_2-16 at. % Ag film was exposed in AO for in long-term. 2H-MoS_xO_y matrix was oxidized to MoO_3 and MoO_2, and alloyed Ag partially to Ag_2O which led to cracking and decrease of wear resistance of MoS_2-Ag composite film.	Gao et al., 2018
Deposition of multilayer $Ti_3C_2T_x$ coatings stainless steel by electrospraying	Exploited the thermally/mechanically degraded MXenes and amorphous/nanocrystalline iron oxides formation having utilised ball-on-disk tribometry (Si_3N_4 counterbody) with acting contact pressures of about 300 MPa.	Compared to 2D nanomaterials, MXene-coated specimens demonstrate a 6-fold friction reduction and an ultralow wear rate (4×10^{-9} mm^3 N^{-1} m^{-1}) over 100 000 sliding cycles, giving 200% better wear life.	Grutzmacher et al., 2022
Surface Texturing			
2–7 μm, Line- and cross-like microstructures DLC layers on steel surface.	Technique produced a 5 μm crater-like structures with a 50 μm layout interval.	Wear reduction is greatly improved by direct laser interference patterning. Friction decreased from the initial DLC layers' friction coefficient of 0.18 to 0.11.	[Jahnig and Lasagni, 2020; Zwahr et *al.*, 2019]
Dimple in Si3N4 mated with steel.	Examined the effects of dimple size and density with sliding tests.	Sample achieved a surface wear reduction of up to 72% based on a 5% dimple area percentage.	[Tang et *al.*, 2013; Wakuda et *al.*, 2003]

Deposition of DLC layer on duplex treated Plasma nitrocarburized, quenched and tempered H13 steel.	Utilzing physical vapor deposition (PVD) and plasma-enhanced chemical vapor deposition (PECVD), chromium nitride (CrN) and diamond-like carbon layer of different thicknesses were deposited one after the other.	Thickest CrN and DLC case showed higher hardness and better tribological properties, however, they failed under brittle condition.	Condea et al., 2019
DLC-covered textured surface with dimple.	Examined anti-wear effect of dimple density on sample under 820 MPa of contact stress.	Comparing the sample with a 44 percent dimple density, the sample with 24 percent dimple density had less wear rate but has an elevated friction coefficient.	[Ghosh et *al.*, 2015]
Synthesized Cr/CrN/(Cr,N)-DLC/DLC and Cr/Cr-DLC/DLC multilayer coatings using DC sputtering magnetron technique	Utilized a deposition pressure in the range of 0.3 to 0.5 Pa to sputter chromium and graphite targets to achieve a dense and compact structure with sharp interfaces.	Global coating adhesion on stainless steel and hardness were improved due to Cr (N) and Cr-DLC multilayers deposition on DLC coatings.	Duminica et al., 2018.
Surface Hardening			
Alloying Ti surfaces by plasma diffusion technique for surface hardening	Used hardening technique to form a robust surface film, enhancing wear resistance on sample	Anti-wear properties of Ti-based alloy surfaces was enhanced by the formation of TiN, TiC, and hard Ti-based intermetallics surface film.	[Kim et *al.*, 2003]
Duplex surface & subsurface hardening of M50 steel	Used technique comprising traditional hardening and surface nitriding treatments to prevent wear.	The subsurface residual compressive stresses improvement enabled superior anti-wear.	[Budinski, 1993]
Pulsed electron beam technique of CrFeCoN-iMo hardening.	Utilized sample hardening to exploit the impact of elevated density craters, ultra-fine grains,	Wear resistance and hardness were attained by achieved by raising the surface's pulse count to	[Lyu et *al.*, 2020]

	dislocations, and warped twins.	fortify the underlying mechanisms	
Hydrophobic surfaces hardening of Steel for wear resistance	Used low-temperature plasma surface alloying and fabrication of super-hydrophobicity channel-like textures to harden steel.	Hardening of steel surface improved from 172 to 305 HV. After plasma carburizing, surfacing durability was found to be between 28 and 59 percent.	[Garcia-Giron et *al.*, 2019]
Architecture			
Rung-stepped microstructure modification and passive nano-particle layer on Aluminum (Al) surface.	Used micro and nanoscale binary hierarchical modified microstructure tribo-layer technique employs to aid wear reduction.	Hierarchical surface's wear resistance rate decreased from 1.49×10^{-5} mm and $2N^{-1}$ for the unprocessed Aluminum surface to 0.89×10^{-5}mm and $2N^{-1}$.	[Li et *al.*, 2016]
Hierarchical structure-replacement of Aluminum cathode with graphite and Al^{3+} tailoring.	Used a dense-surface layer, a permeable sub-layer and an impediment layer by formation of columnar wear debris.	The adapted sample wear rate was 3 times magnitude lower than that of the untreated Aluminum, and the hardness of the refined surface was 2–7 times of original aluminum alloy.	[Wu et *al.*, 2016]
Prepared a super wear-resistant superhydrophobic surface with hierarchical structure	Utilized wire electrical discharge machining (WEDM) to obtain the maximum apparent contact angle (ACA) and best triangular surface texture.	micron-grade discharge morphology and the absorbed organics can increase apparent contact angle from 75.5° to 121°	Chen et al., 2022

2.1 Matrix Composition Strengthening

Material properties can be altered by blending additives to the base or by enhancing the manufacturing and post-treatment processes. This includes application of 2D-nanoparticles at micro and nanoscales in nano-phase compositions, such as nanocomposites, optimization and post-treatments. To lessen material structural damage and surface asperity during interactions, dopants are widely used to create components that are resistant to wear [Chan et al., 2018]. They have a substantial impact on metal materials' lattice distortion, fracture performance, plasticity, and bonding strength, influencing wear resistance. Some processes are illustrated below in Table 5:

Table 5: Wear Reduction by Strengthening Composition

Material & Method	**Sample Characteristics**	**Test Observation/Remark**	**Ref**

Composition			
Mo doped in fcc CrCoNi alloys	Compressive yield strength and hardness were achieved with this technique, ranging from 518 MPa at 244 HV to 1973 MPa at 656 HV.	Technique led to lattice distortion and development of intermetallic phases, However, synthesized CrCoNiMo0.5 had good anti-wear and mechanical characteristics.	[Miao et *al.*, 2018]
AZ91 alloys doped La-based rare earth	The phase microstructure of the doped alloys was altered from the basic AZ91 alloy's continuous network to its spherical form.	As temperature rose from 25 °C to 200 °C, doped alloys' microstructure wear resistance was enhanced.	[Zafari et *al.*, 2013]
Tuning $B^{1-x}C^{x}$ films on Si (100) and steel substrates surfaces	Technique created a graphitic tribolayer by manipulating the magnetron system's electrical power, which caused the development of amorphous carbon in $B^{1-x}C^{x}$ films.	Hardness measurements of $B^{1-x}C^{x}$ sheets revealed values of 28, 20, and 25 GPa, or 19, 56, and 76 percent carbon content, respectively. With more carbon present, the wear rate fell almost two orders of magnitude.	[Qian et *al.*, 2015]
Ag doped with Al elemental proportion to form $Ag^{1-x}Al^{x}$ alloys.	At above 25 %, Al content produced the hexagonal close-packed (hcp) phase tuning as a foundation for creating the ideal doping composition.	Increase in Al content enhanced $Ag^{1-x}Al^{x}$ alloys' hardness because the fcc phase has elevated slips than the hcp phase. Compared to pure silver and alloys with other phases, this demonstrated stronger anti-wear properties.	[Taher et *al.*, 2018]
Microstructure			
0.4 to 2.2 μm on the wear resistance of WC-Co materials.	Anti-wear was observed at dry sliding and micro-abrasion conditions.	wear rate was reduced by decreasing the WC grain size to obtain increased hardness which lessened surface deformation, fracture, and oxidation, reducing wear rate.	[Wang et *al.*, 2019]
macroscale wear resistance of NiTi alloys with grain sizes ranging from 3 to 80 nm	Grain size was evaluated under various normal loading and wear resistance of Ni-W alloys.	The nanocrystalline NiTi alloys' anti-wear performance was primarily influenced by their hardness. Ni-W alloys had greater wear resistance than the 3 nm average grain size value.	[Liu et *al.*, 2019]

Ni-based composites doped with 1 wt% CNTs.	Examined grain refinement process using hot uniaxial press technique	Reduction in grain size of pure Ni metals from 47.54 μm, to 7.58 μm of CNT-reinforced composites led to composites' increased hardness and subsequent high wear resistance.	[Suarez et *al.*, 2014]
Inverse Hall–Petch relation of the CoCrFeMnNi alloy	Process was demonstrated in an inert non-oxidation environment.	In coarse-grained alloys, a low wear rate was observed. This was linked to the development of near-amorphous layer with severely deformed surface.	[Jones et *al.*, 2020]
Steel structures of various grain sizes, comprising 4 μm, 18 μm, and a bimodal grain-size distribution.	Process investigated strain hardening effect and various harmonic heterogeneous lamellar structures	Due to the fine and strained grain effect of the heterogeneous structure, bimodal grain size steel provided the maximum wear resistance.	[Rai et *al.*, 2018]
Reinforcements			
Pristine and functionalized graphene additives (modified-graphene reinforced polymers).	Molecular dynamics simulation of pristine and functionalized graphene additives during precipitation and grain boundary hardening was examined.	Sample showed 42.3% wear reduction in modified-graphene reinforced polymers. Combination of reinforcements and ultra-fine grain microstructures enhanced anti-wear property of metallic materials.	[Li et *al.*, 2017]
Laser engineered net shaping of Ni-18Al-11Cr-9C and Ni-14Al-8Cr-29C alloys.	Process precipitates nickel aluminide and chromium carbide in samples. And the carbon content impact was examined in the alloy.	Wear was reduced in worn alloys by a phase change from grains to nano-crystalline tribolayers caused by SPD. Wear rate at 29% was decreased. .	[Mohseni et *al.*, 2015; Torgerson et *al.*, 2019]

3. Wear Reduction in Automotive Materials

The universal energy utilization to overcome friction is estimated at 32% of approximate 83 EJ in road vehicle sector and 30% approximate in other transport sectors, annually. According to Holmberg and Erdemir, (2017), energy consumption based on wear accounts for 10% of frictional energy percentage. According to Gullino et al., (2019), all of these may be ascribed to the use of

regularly used transport vehicle materials, steel and aluminum alloys, which were chosen for their suitable mechanical capabilities and affordable price. It is possible to reduce the frequency of component replacements and remanufacturing by developing and using materials for transportation that have greater wear-resistance and lubricating systems that limit wear loss for vehicles [Erdemir and Holmberg, 2015]. Several of the most modern anti-wear structures and materials, including AM metallic materials are resorted to due to their suitable tractability in designs and manufacture [Holmberg, 2012]. For instance, Wang et al., (2018) produced austenitic 316L stainless steel having higher yield strength and tensile ductility than the standard 316L steel, which in normal case, increased in strength, but caused a decline in ductility. It was determined that the distinctive cellular architectures, low-angle grain region, and AM-induced dislocations were the causes of the high yield strength. It was determined that the distinctive cellular architectures, low-angle grain boundaries, and AM-induced reformation were the causes of the high yield strength. The higher ductility was associated with the development of hierarchically heterogeneous microstructures, which led to the gradual and progressive strain hardening. In order to improve the wear resistance of metallic materials, the impact of reformations and gradual strain hardening are crucial. Additionally, the insertion of zirconium nanoparticles crystal nuclei into the AM production of seamless aluminum alloys with good-grain microstructures which results in high strengths that were on par with their wrought counterparts [Martin et al., 2017]. It has been observed that zirconium nanoparticles favorably react with Aluminum in the melting pool to generate the Al3Zr phase, this has over 20 identical interfaces with the aluminum phase, giving low energy nucleation spots. This is because AM technique uses a high cooling rate and frequent thermal cycling. Ti-based alloys with ultrafine eutectoid microstructures could be produced with an excellent balance of high strength and ductility. In the manufacture of intricately formed car components, where solidification cracking is frequently seen in conventional AM techniques. Another important supplementary process to conventional heat treatment method for wear, austenite and cost reduction is the cryogenic treatment process. Although, automotive heat treatments employed processing temperature greater than 273 K, however, last century has witnessed utilization of subzero treatment; cryogenic treatments [Jovicevic-Klug et al., 2020]. Cryogenic treatment is classified into;

i. Conventional cryogenic heat treatment, at $-80 \leq$ temperature $\leq 0\ ^{o}C$, [Jovicevic-Klug et al., 2020].
ii. Shallow cryogenic heat treatment, at $-80 \geq$ temperature $\geq -160\ ^{o}C$, [Jovicevic-Klug et al., 2021; Senthilkumar, 2016].
iii. Deep cryogenic heat treatment at temperature $< -160\ ^{o}C$, [Jovicevic-Klug et al., 2021; Ciski et al., 2019].

Where ‘t’ represents temperature.

Additionally, deep cryogenic treatment causes a microstructural changes of reduction in carbides size, generating a homogenized carbide distribution [Li et al., 2018]due to jumping of carbon atoms to neighboring sites at lower temperature to the high degree of contraction in the ferrous structure for eta chromium carbide nucleation [Amini et al., 2012; Paydar et al., 2014; Amini et al., 2014].Cryogenic heat treatment enhancement are essential in tools like gears, brakes, rotors, bearings, pinion shafts, crown wheels and dies [Baldissera 2009], with deep cryogenic heat

treatment finding application in various ferrous materials, such as; carburized steels [Baldissera and Delprete, 2009], high speed steels [Firouzdor, 2008] and tool steels [Akhbarizadeh et al., 2013]. The impact of cryogenic heat treatment in some materials is briefly highlighted in Table 6. Cryogenic treatment refines grain characteristic of materials.

Table 6: Effect of Cryogenic heat treatment in materials

S/N	Material/Composition	Enhancement	Remark	Refs
1	Impact of DCT on friction and wear performance of high-speed steels (AISI M2, AISI M3:2 and AISI M35)	DCT improves its abrasive wear resistance under high sliding speed conditions within 30–60%. And 25% enhancement than CHT.	Coefficient of friction and wear rate of CHT and DCT heat-treated HSS (AISI M2, AISI M3:2 and AISI M35) tested under recipro-cating dry sliding con-ditions against Al2O3 ball.	Jovicevic-Klug et al., 2021
2	Conducted DCT effect on steels: AISI M2, M3:2 and M35, utilizing XPS for breakdown of their oxidation dynamics.	Precipitated carbides increased for DCT samples by 17%, 4% and 25% for steels M2, M3:2 and M35, respectively.	DCT impacted both carbide precipitation and the matrix by generating a finer micro-structure and smoother surface formation.	Jovicevic-Klug et al., 2021
3	Impact of effect of surface finishing on on corrosion behavior of steel AISI M35 by DCT AND CHT comparison.	DCT had 26 % and 13% lower pits com-pared to CHT by for 1 day and 7 days of immersion. DCT has potential to prolong AISI M35 lifetime in corrosive media, such as saltwater.	Samples were polished, etched and immersed in LN_2. Nitrogen-based surface finish significantly suppressed the development of corrosion products by formation of green rust.	Jovicevic-Klug et al., 2021
4	Impact of tempering in DCT of AISI M35 high-speed steel	Maximum carbide precipitation was reached at 550 °C and highest hardness of 880.4 HV_1 was obtained at 150 °C of specimen tempering.	Impact toughness of the sample tempered at 550 °C was the best at 2.50 MJ m^{-2}, which is due to an increase in the number of martensite block boundaries and more homogeneous carbide precipitation.	[Xu et al., 2022]
5	Optimum heat treatment process parameters of	Best abrasive wear resistance occurred at 1200 °C of DCT applied before	Samples were austenitized at 1170, 1200 or 1230 °C and quenched in salt bath via	Fantineli et al., 2020.

	cryogenic treatments of AISI M2 samples.	double tempering. DCT enhances wear resistance of the AISI M2 steel by selecting proper heat and CTs parameters.	nitrogen nebulization (CT process) with a cooling/ heating rate of 0.3 °C/min, and 24-h holding time at −190 °C.	
6	Hardness and its damping capacity of M2 steel was examined for nano-scratch testing.	Wear resistance increased in the quenched samples by DCT based on austenite-martensite conversion during cooling. However, prolonged isothermal cryogenic treatment is not beneficial to M2 HSS frictional properties.	Oil quenching was conducted on samples and DCT immersion was carried out in liquid nitrogen for 1, 5, 24, 48 h, or 120 h. The samples were mounted in epoxy, sanded with emery paper of 600 grit size, polished with ultra-fine metallographic paper and diamond suspension.	Zhou et al., 2019
7	Hierarchical microstructure and strength-toughness of M54 SH-UHSS was examined for influence of cooling rate during CT	Cooling rate refined martensite matrix and M2C-type (M = Mo, Cr, W, V) carbides at 3 °C·min^{-1}.	Refined blocks martensitic matrix precipitation was identified to give impact toughness (30J) with ultra-high strength (1730 MPa yield strength and 2018 MPa ultimate tensile strength).	[Zhang et al., 2022]
8	Impact of cryogenic treatment on microstructure, hardness, red hardness and wear resistance of M35 high speed steel (HSS)	The grain size and irregular bulk carbides are reduced after DCT, and a large number of spherical carbides with sizes less than 1 μm were precipitated within the grain.	Best wear resistance with refined grain size and wear volume reduction was achieved by deep cryogenic treatment (DCT) at 525℃. Increase in tempering temperature caused a decrease in the residual austenite in M35 HSS.	[Bi et al., 2021]
9	Examine Tungsten carbide (WC-Co)	Wear behavior of WC-Co tools improved at low	Improvement is attributed to formation of an improved new eta (η)	[Sreerama Reddy et al., 2009;

	cutting tool phase consisting of; i. Alpha (α–phase) ii. Beta (β- phase) iii. Gamma (γ-phase) iv. Eta (η-phase)	temperatures and not long working cycles	carbides phase and decrease in the beta (β) phase, during cryogenic treatment.	Vadivel and Rudramoorthy, 2009]
10	Impact of nitrogen in DCT of ISI M35 Alloy, related to nduced surface chemistry changes.	DCT samples showed modified thickness, compos-ition and structured layers of corrosion products and passive film compared to CHT sample under the same environment-al conditions.	Utilized 24 h soaking time and -196 ^{o}C soaking temperature with emphasis on time-of-flight secondary ion mass spectroscopy (ToF-SIMS) in corrosion behavior of sample.	[Jovicevic-Klug et al., 2020]
11	CT impact on retained austenite (RA) evolution and mechanical properties of 55Cr17Mo1VN plastic die steel.	Treated sample showed excellent tensile strength (~2241 MPa) and high hardness (~56.2 HRC) leading to precipitation, fine grain and dislocation strengthenings.	After CT, RA volume fraction decreased from 44.7 to 35.4%, while the hardness increased from 39.0 to 54.6 HRC because of the increase in the dislocation density.	[Kang et al., 2021]
12	CT impact on Magnesium alloys (AZ91). *Consisting of;* i. HCP magnesium phase (α phase) ii. BCC intermetallic compound of Mg17Al12 (β phase).	Cryogenic treatment of AZ91 after casting enhanced mechanical properties and corrosion resistance of AZ91	Enhancement was due to the change in the β phase distribution after the cryogenic treatment. Deep cryogenic heat treatment slightly enhanced the hardness and wear behavior of the AZ91 alloy microstructure.	[Amini et al., 2014; Yong et al., 2012].
13	Effectiveness of DCT on three different chemical composition of high-speed steels (HSS) (AISI M2, AISI M3:2 and AISI M35).	DCT enhanced the hardness, fatigue resistance, compressive strength and strain hardening of the HSS, promoting homogenous	Level of improvement via DCT effect depended on heat treatment conditions (lower austenitization and higher tempering temperature).	Jovicevic-Klug et al., 2022

		microstructure and more carbide precipitation (∼40%).		
14	DCT impact on Titanium alloys (i.e., Ti-6246 and Ti– 6Al–4V).	Deep cryogenic heat treatment improved hardness and lowered the wear rate of the titanium alloys. It lowered the friction coefficient of the Ti-6Al-4V alloys.	This enhancement is achieved at longer durations of deep cryogenic temperatures with a reduction in grain size and the β-phase (high degree of contraction).	[Gu et al., 2014]
15	Carburized 20CrNi2MoV steel cryogenically treated: i. cryogenic treatment at −80 ◦C (CT) ii. deep cryogenic treatment at −196 ◦C (DCT)) iii. conventional heat treatment (CHT) on	DCT precipitated more of fine carbides which plays a more prominent role in enhancing wear resistance.	Wear resistance of sample steel was improved by 17% due to CT and by 25.5% due to DCT when compared to CHT. Wear resistance was attributed to microstructural changes: finer martensitic structure, reduced retention of austenite and carbide development.	[Li et al., 2018]

3.1 Surface Engineering, tribology and Tribo-corrosion of Automotive Parts

The control of mechanical and tribological properties of surfaces employs surface engineering techniques like Laser shock peening (LSP), and Ni/GPL nanocomposite coatings, and such engineered surfaces exhibit tribo-corrosion behavior [Siddaiah et al., 2018; Nazir et al., 2018]. Tribo-corrosion (corrosion and wear) of automotive parts is prevalent due to the simultaneous actions of both mechanical and chemical reaction. The solution to this issue has been reported to be the application of a liquid lubricant containing suitable additives and suitable surface coating on the substrate to improve the wear resistance and corrosion resistance of the automotive parts as highlighted in Table 7. Tribo-corrosion causes failure of components which results in the replacement of parts and a reduction in the productivity of machines. Most automotive bodies are made of steel sheets **a**nd notable related researches on anti-wears are briefly highlighted in Table 7.

Table 7: Tribo-corrosion in Automotive Parts Materials

S/N	Study	Process Utilized	Remark	References
1	Corrosion of steel sheet due to quality of surface pickling solution.	Utilized pretreatment phosphating as a tool in corrosion resistance of AHSS	Utilized HNO3-based pickling condition in phosphate coating-film adhesion	Cho et al., 2021

2	To enhance the working performance of H13 steel by multi-phase coating.	Introduced multi-phase, intermetallic compounds (Fe, Mo and Cr) to generate coating hardness of approxima-tely 1400 HV with good wear resistance 7 times higher than the substrate	Utilized electro-spark deposition, discharge frequencies and specific deposition to improve the hardness, wear resistance and corrosion resistance of Mo coatings on H13 mould steel.	Wang et al., 2021
3	Protection of stainless steel from oxidation at temperatures up to 950 ^{o}C through hydrothermal processing.	Utilized polymer-derived ceramic (PDC) synthesis route to synthesize better ternary composite polycrystalline coating (Al2O3-Y2O3-ZrO2)	Examined degradation mechanisms of coatings during various stages of the hydrothermal process, producing composite which can withstand harsh environmental conditions	Parchovianská et al., 2021; Parchovianská et al., 2021.
4	Examined the structure, mechanical properties, corrosion, and tribocorrosion behavior of stainless-steel.	Used a filtered cathodic vacuum arc (FCVA) system by adjusting bias voltage on Ti-DLC coatings of steel substrate.	Increase in bias voltage from −50 to −200 V led to hardness increase from 30.23 GPa to 34.24 GPa in Ti-DLC coatings, while best anti-tribocorrosion result of 0.052 smallest friction coefficient and 2.48 × 10−7 mm3/N·m wear rate was obtained at −200 V.	Shen et al., 2022
5	Laser shock peening (LSP) surface modification processes of 1045 steel	Investigated the impact of laser intensity on surface roughness and its effect on the coefficient of friction (COF) and transfer layer formation using LSP	When laser intensity is increased, COF decreased due to surface strengthening and roughening effects to a threshold value, and beyond the threshold, it increased as a result of the dominant surface roughening effect.	Siddaiah et al., 2018
6	Compared the synergistic wear-corrosion performance of	Utilized Archard model with nano-mechanics and electrochemistry for Ni/GPL and steel 1020	Analysis and modelling reveal that the synergistic wear-corrosion effects were	Nazir et al., 2018

	Nickel-Graphene (Ni/GPL) nanocomposite coating with un-coated steel 1020 under reciprocating-sliding contact	while noting the effect of applied wear-corrosion in both samples.	majorly prominent in steel compared to Ni/GPL particularly under contaminated lubricating oil conditions with Ni/GPL exhibiting less severe micro-ploughing due to refined grain structure.	
7	Examined the impact of LSP surface processing on wear-corrosion behavior of AZ31B Mg alloy	Utilized a zero-resistance ammeter (ZRA) technique to determine the evolution of open circuit potential during wear-corrosion analysis.	Wear-accelerated corrosion during sliding was mitigated by LSP processing due to decrease in the corrosion potential difference between worn and unworn regions of the surface.	Siddaiah et al., 2019
8	Examined different LSP impacts on the mechanical properties in artificial seawater and corrosion resistance of shipbuilding 5083Al alloy	Utilized a ball-on-disk sliding wear tester and electrochemical workstation in n 3.5% NaCl solution.	Electrochemical corrosion rate of the treated samples decreased by 74.91% and 95.03% after being treated by 1 and 3 LSP impacts compared with the untreated sample.	Wang et al., 2018
9	Investigated the tribological behavior and inherent features of the DLC coatings as a function of deposition conditions	Employed Diamond-Like Carbon (DLC) deposition by pulsed DC Plasma Assisted Chemical Vapor Deposition (PACVD) technique.	Feeding gas “H/C” ratio and temperature increase up to certain values played a dominant role in the hardness and elastic modulus increase and reduction of wear rate than their diverse intrinsic properties.	Jokari et al., 2017
10	Fabricated a stearic acid modified-superhydrophobic cobalt-graphene, Co-G, composite films on a steel substrate	Employed Potentiostatic deposition of cobalt film and cobalt-graphene, Co-G, composite, followed by modification with low surface energy stearic acid (SA).	They noted that Co-G-SA film shows a higher roughness due to the network structures of graphene, hence, exhibited higher super-hydrophobicity. corrosion current	Mohamed and Abd-El-Nabey, 2022

			density for Co-G-SA, Co-SA films and bare steel were 0.1732 µA, 0.7094 µA and 0.1457 mA, respectively.	

4. Conclusion

A review of characteristics, test devices and wear reduction in automotive application has been provided. Development of alternative laboratory-scale testers to ascertain variability in instrumentation and measurement for repeatability and reproducibility in-line with ASTM standards and modification is essential for better manufacturing operations. This way, changes in wear as a function of time, varied loads and liner materials can be ascertained in practice. Improvements made to enhance test device efficiencies and lower wear rates includes materials of the test device, for example, utilizing 2D materials under prolonged timeframe conditions has its impact, therefore, exploiting nanoparticles for its excellent micro- and nanoscale anti-wear characteristics is essential, since nanoparticles possess good anti-wear capabilities even at extended timescale conditions. Moreso, nano-phase compositions will have better wear resistance based on parametric optimization, preparation, and post-treatment. Modeling and simulation of nanostructures reproducibility and stability is essential in describing the basic mechanisms of wear-resistant nano-structure, designs and phase transformations, aiding theoretical understanding of additive manufacturing (AM) metallic materials with nanocrystalline and twinned features, AM unstructured materials, and AM elevated-entropy alloys as anti-wear materials with excellent mechanical properties.

Generally, wear can be effectively controlled by designing microstructures (hierarchical or heterogeneous surface structure designs), controlling compositions (additives in matrix or parameter fabrication and post-treatment processes optimization), and introducing reinforcements (precipitates and second-phase particles). Other peculiarity in wear reduction in automotive materials;

- Introduction of surface texturing, coatings, on substrate surface generates superior tribological behaviors, and dopants are introduced in matrix composition strengthening to reinforce plasticity, bonding strength and influence anti-wear.
- Cryogenic treatment (particularly deep cryogenic treatment) enhances mechanical properties, thereby reducing residual stress and coefficient of friction, improve anti-wear, hardness, toughness and fatigue resistance.
- Pretreatments like Laser shock peening can cause considerable reduction in electrochemical corrosion (~80%).

4.1 Recommendation

Robust analysis can be conducted by adding a temperature and humidity sensor device interfaced with digital user interface to measure parametric wear and friction variations in developed wear testing systems. This will make measurement of dynamic loading and unloading impact on wear

rate easier to analyze. Finally, experimental investigations, modeling, and theoretical simulations on super-lubricity in industrial and energy applications at high temperatures, elevated pressures, variable speeds, high loads, and vacuum conditions may contribute to a more comprehensive understanding of wear behavior, development of test devices and applications especially in automotive parts.

References

1. Rosenkranz, A., Grützmacher, P.G., Gachot C. and Costa, H.L. (2019). Surface Texturing in Machine Elements - A Critical Discussion for Rolling and Sliding Contacts. Adv Eng Mater., 21(8): 1-20.
2. Rosenkranz, A., Costa, H.L., Baykara, M.Z. and Martini, A. (2021). Synergetic effects of surface texturing and solid lubricants to tailor friction and wear - a review. Tribol. Int., 155: 1-21.
3. Gachot, C., Rosenkranz, A., Hsu, S. and Costa H. (2017). A critical assessment of surface texturing for friction and wear improvement. Wear, 372: 21–41.
4. Koszela, W., Pawlus, P., Reizer, R. and Liskiewicz, T. (2018). The combined effect of surface texturing and DLC coating on the functional properties of internal combustion engines Tribol. Int., 127: 470–477.
5. Rosenkranz, A., Costa H.L., Profito, F., Gachot, C., Medina, S. and Dini, D. (2019). Influence of surface texturing on hydrodynamic friction in plane converging bearings - An experimental and numerical approach. Tribol Int., 134:190–204.
6. Profito, F.J., Vlădescu, S.C., Reddyhoff T. and Dini D. (2017). Transient experimental and modeling studies of laser-textured micro-grooved surfaces with a focus on piston-ring cylinder liner contacts. Tribol Int., 113:125– 136.
7. Zimmer, M., Vlădescu S-C, Mattsson L, Fowell M and Reddyhoff T. (2021). Shear-area variation: A mechanism that reduces hydrodynamic friction in macro-textured piston ring liner contacts. Tribol Int., 161: 1-16.
8. Wang, B., Zheng, M., and Zhang, W. (2020). Analysis and Prediction of Wear Performance of Different Topography Surface. Materials (Basel), 13(22): 5056-5071.
9. Calderon, C.D.R., Cazares, I., Galicia, D.L.S. and Cabrera, L.I.F. (2022). Method for conducting micro-abrasion wear testing of materials in oscillating sliding. MethodsX, 9:101703-14.
10. Hareesha, M. and Jeevan, T.P. (2014). Modification of Abrasive Wear Testing Machine and Testing of Materials. International Journal of Science and Research, 3(10): 2319-7064.
11. Psyllaki, P.P. (2019). An Introduction to Wear Degradation Mechanisms of Surface-Protected Metallic Components. Metals, 9: 1057-1074
12. Patrick, J.F., Robb, M.J., Sottos, N.R., Moore, J.S. and White, S.R. (2016). Polymers with autonomous life-cycle control. Nature, 540: 363-370.
13. Parande, G., Manakari, V., Meenashisundaram, G.K. and Gupta, M. (2016). Enhancing the hardness/compression/damping response of magnesium by reinforcing with biocompatible silica nanoparticulates. Int. J. Mater. Res., 107: 1091-13.

14. Gullino, A., Matteis, P. and D'Aiuto, F. (2019). Review of Aluminum-To-Steel Welding Technologies for Car-Body Applications. *Metals*, 9: 1-25.
15. ASTM Standard, G76-95 (1995). Standard Practice for Conducting Erosion Tests by Solid Particle Impingement Using Gas Jets, Annual Book of ASTM Standards, 3(2): 321-325, ASTM, Philadelphia.
16. Prabhu P., Suresh Kumar M., Singh A.P. and Siva K. (2014). Experimental Study and Verification of Wear for Glass Reinforced Polymer using ANSYS. Global Journal of Researches in Engineering: A Mechanical and Mechanics Engineering. 14(3): 1-13.
17. Bayer, R.G. (2002). Wear analysis for engineers. HNB Publishers, New York. Pp.: 1-360. ISBN: 096642865X.
18. Reniel E.Y., Luis N.H., Omar Z.M., Nelson C.O. and Acacio, F.N. (2014). Design and fabrication of a machine for test in abrasive wearing according to ASTM G65 standard. American Journal of Materials Science and Application, 2(5): 86-90.
19. Nassar, A.E. and Nassar, E.E. (2011). Design and fabrication of a wear testing machine. Leonardo Electronic Journal of Practices and Technologies, 19: 39-48.
20. Ogedengbe, T.S., Yussouff, A.A. and Adanikin A. (2018). design and development of a wear testing machine for manufacturing laboratories. 1st fuoye international engineering conference. Pp. 77-86.
21. Govind, G., Henckel, J., Hothi, H., Sabah, S., Skinner, J. and Hart, A. (2015) Method for the location of primary wear scars from retrieved metal on metal hip replacements. BMC Musculoskeletal Disorders, 16: 1-5.
22. ASTM G99-95a (1997). Standard test method for wear testing with a pin-on-disc apparatus, Annual Book of ASTM Standards, 03.02(1997)392-396.
23. ASTM G133-95, standard test method for linearly reciprocating ball-on-flat sliding wear, Annual Book of ASTM Standards, 03.02(1997)529-536.
24. Lin, C.L., Fallahnezhad, K., Brinji, O. and Meehan, P.A. (2022). Mitigation of False Brinelling in a Roller Bearing: A Case Study of Four Types of Greases. *Tribol Lett*, 70 (1): 1-22
25. Balic, E.E and Blanchet, T.A. (2005). 15th International Conference on Wear of Materials: Editors: Blau, P. and Shaffer, S.L., Part II. April 24-28, San-Deigo, California, 259:876-881
26. ASTM G76-95, (1997). Standard test method for conducting erosion tests by solid particle impingement using gas jets, Annual Book of ASTM Standards. Pp. 305-309
27. ASTM G65-94 (1997). Standard test method for measuring abrasion using the dry sand / rubber wheel apparatus, Annual Book of ASTM Standards. Pp. 239-250
28. ASTM B611-85 (1995). Standard test method for the abrasive wear resistance of cemented carbides, Annual Book of ASTM Standards. Pp. 326-327.
29. ASTM G105-89 (1997). Standard test method for conducting wet sand/ rubber wheel tests, Annual Book of ASTM Standards. Pp. 424-432.
30. Pinto, G.F., Baptista, A., Silva, F., Porteiro, J., Miguez J. and Alexandre, R. (2021). Study on the Influence of the Ball Material on Abrasive Particles' Dynamics in Ball-Cratering Thin Coatings Wear Tests. Materials, 14(3): 1-28.
31. Yousif, I.F. and Ataiwi, A.H. (2018). Construction of slurry jet erosion tester and the effect of particle size on slurry erosion. Kufa Journal of Engineering, 9(3): 17-25.
32. Pilliar, R.M. (2009). Metallic Biomaterials: In Biomedical materials, N. Roger, Ed. Springer Springer Science and Business Media: New York, NY, USA. Pp. 41-81.

33. Suresh, K.S.; Geetha, M.; Richard, C., Landoulsi, J., Ramasawmy, H., Suwas, S.,Asokamani, R. (2012). Effect of equal channel angular extrusion on wear and corrosion behavior of the orthopedic Ti-13Nb-13Zr alloy in simulated body fluid. Mater. Sci. Eng. C, 32: 763–771.
34. Bhushan, B. (2008). Nanotribology, nanomechanics and nanomaterials characterization. Philos. Trans. R. Soc. A, 366: 1351–1381.
35. Zhou, K. and Liu, B.O. (2022). Molecular dynamics simulation: Fundamentals and Applications. 1st Edition, Elsevier, eBook ISBN: 9780128166161.
36. Tayebi, N., Zhang, Y., Chen, R. J., Tran, Q. and Chen, R. (2010). An Ultraclean Tip-Wear Reduction Scheme for Ultrahigh Density Scanning Probe-based Data Storage. ACS Nano, 4(10): 5713-5720.
37. Fletcher, P.C., Felts, J.R., Dai, Z., Jacobs, T.D. and Zeng, H. (2010). Wear-Resistant Diamond Nanoprobe Tips with Integrated Silicon Heater for Tip-based Nanomanufacturing. ACS Nano, 4(6): 3338-3344.
38. Jacobs, T.D. and Carpick, R.W. (2013). Nanoscale Wear as a Stress-Assisted Chemical Reaction. Nature Nanotechnology, 8(2): 108-112.
39. Killgore, J.P., Geiss, R.H. and Hurley, D.C. (2011). Continuous Measurement of Atomic Force Microscope Tip Wear by Contact Resonance Force Microscopy. small, 7 (8): 1018–1022.
40. Liu, J., Notbohm, J.K., Carpick, R.W., and Turner, K.T. (2010). Method for Characterizing Nanoscale Wear of Atomic Force Microscope Tips. ACS Nano, 4(7): 3763-3772.
41. Liu, J., Grierson, D.S. Moldovan, N., Notbohm, J. and Li, S. (2010). Preventing Nanoscale Wear of Atomic Force Microscopy Tips through the Use of Monolithic Ultra-nanocrystalline Diamond Probes. Small, 6(10): 1140-1149.
42. Tinnemann, V., Hernandez, L., Fischer, S., Arzt, E., Bennewitz, R. and Hensel, R. (2019). In Situ Observation Reveals Local Detachment Mechanisms and Suction Effects in Micropatterned Adhesives. Advanced Functional Materials, 29(14): 1-11.
43. Tian, F., Qian, X., and Villarrubia, J. (2008). Blind Estimation of General Tip Shape in AFM Imaging. Ultramicroscopy, 109(1): 44-53.
44. Luka, S., Franci, P. and Mitjan K. (2019). Determination of friction coefficient in cutting processes: comparison between open and closed tribometers. Procedia CIRP 82:101-106.
45. Abadias, G., Chason, E., Keckes, J., Sebastiani, M., Thompson, G., Barthel, E., Doll, G., Murray, C., Stoessel, C. and Martinu L. (2018). Review Article: Stress in thin films and coatings: Current status, challenges, and prospects. Journal of Vacuum Science & Technology A., 36(2): 020801- 48.
46. Jibran, W., Hogan, J.D. and Mcdonald A. (2021). Influence of Spray Parameters on the Thickness, Hardness and Porosity of low-pressure Cold Sprayed WC-Ni Coatings. Research Square, 2021: 1-20.
47. Lin, Q.Y., Wei, Z.Y., Wang, N. and Chen, W. (2013). Analysis on the lubrication performances of journal bearing system using computational fluid dynamics and fluid–structure interaction considering thermal influence and cavitation. Tribology International 64:8–15.
48. Li Q., Wang, Y.J., Zhang, S., Xu, W.W. and Wang, Z.B. (2019). Investigation on hydrodynamic superposition loading mechanism and micro-hydrodynamic effect of textured water-lubricated bearings. Surface Technology, 48: 180.

49. Klimczak, T. and Jonasson, M. (1994). Analysis of real contact area and change of surface texture on deep drawn steel sheets. Wear, 179, 129-135.
50. Krupka, I. (2013). Measurement of Pressure Distribution: Encyclopedia of Tribology (Eds: Q. J. and Wang, Y.W. Chung), Springer US, Boston, MA 2013, p. 3479. ISBN: 978-0-387-92896-8.
51. Boidi, G., Grutzmacher, P., Kadiric, A., Profito, F., Machado, I. Gachot, C. and Dini, D. (2021). Fast laser surface texturing of spherical samples to improve the frictional performance of elasto-hydrodynamic lubricated contacts. Friction, 9: 1227–1241.
52. Baharin, A.F.S., Ghazali, M.J. and Wahab, J.A. (2016). Laser surface texturing and its contribution to friction and wear reduction: a brief review. Ind. Lubr. Tribol., 68: 57-66.
53. Rosler, F., Gunther, K., Lasagni, A. (2018). In-volume structuring of a bilayered polymer foil using direct laser interference patterning. Appl. Surf. Sci., 440: 1166-1171
54. Bieda, M., Beyer, E. and Lasagni, A. (2010). Direct Fabrication of Hierarchical Microstructures on Metals by Means of Direct Laser Interference Patterning. J. Eng. Mater. Technol., 132(3): 31015-6.
55. Vega, F., Pelaez, R., Kuhn, T., Afonso, C., Recio Sanchez, G. and Martin-Palma, R. (2014). Ultraviolet laser patterning of porous silicon. J. Appl. Phys., 115: 184902-8.
56. Fabris, D., Lasagni, A., Fredel, M. and Henriques, B. (2019). Direct Laser Interference Patterning of Bio-ceramics: A Short Review. Ceramics, 2: 578-586.
57. Fukumura, H., Kohji, Y., Nagasawa, K.-i., Masuhara, H. (1994). Laser Implantation of Pyrene Molecules into Poly (methyl methacrylate) Films. J. Am. Chem. Soc., 116(22): 10304–10305
58. Xing, Y.Z., Wang, G., Zhang, Y., Chen, Y.N. and Dargusch, M. (2017). The effect of surface texturing on reducing the friction and wear of steel under lubricated sliding contact. Int. J. Adv. Manuf. Technol., 93(881): 2327–2335.
59. Ooi, S. and Bhadeshia, H.K.D.H. (2012). Duplex Hardening of Steels for Aeroengine Bearings. ISIJ Int., 52: 1927-1934.
60. Chi, Y., Gu, G., Yu, H. and Chen, C. (2018). Laser surface alloying on aluminum and its alloys: A review. Opt. Lasers Eng., 100: 23-37.
61. Vasudev, H., Singh, G., Bansal, A., Vardhan, S. and Thakur, L. (2019). Microwave heating and its applications in surface engineering: a review. Mater. Res. Express, 6, 102001.
62. Sharma, V., Prakash, U. and Kumar, B.V.M. (2015). Surface Composites by Friction Stir Processing: A Review. J. Mater. Process. Technol., 224: 117-134.
63. Gu W., Qi S., He S. Chu K., Lu Z. and Zhang G. (2022). Different Tribological Behaviors in Multilayer 2D Graphene and 3D Graphene Foam Modified DLC/H-DLC Film in Moist Air. Tribology Letters 70(1):1-16.
64. Chen, W., Fang, B., Zhang, D., Meng, X. and Zhang, S. (2017). Thermal stability and mechanical properties of HVOF/PVD duplex ceramic coatings produced by HVOF and cathodic vacuum arc. Ceram. Int., 43: 7415-7423.
65. Lin, S., Yu, S. and Wu, M. (2008). Effect of Different Coating Materials on Cutting Performance in High-Speed Machining of Mold Steels. Key Eng. Mater., 364–366: 1026-1031.
66. Mutyala K.C., Wu Y.A., Erdemir A. and Sumant A.V. (2019). Graphene - MoS2 ensembles to reduce friction and wear in DLC-Steel contacts. Carbon, 146: 1-16

67. Singh, H., Mutyala, K., Mohseni, H., Scharf, T.W., Evans, R. and Doll, G. (2015). Tribological Performance and Coating Characteristics of Sputter-Deposited Ti-Doped MoS2 in Rolling and Sliding Contact. Tribol. Trans., 58: 767-777.
68. Simmonds, M., Savan, A., Pfluger, E., van swygenhoven, H. (2000). Mechanical and tribological performance of MoS2 co-sputtered composites. Surf. Coat. Technol., 126: 15-24.
69. Ye, M., Zhang, G., Ba, T., Wang, Y., Wang, X. and Liu Z. (2016). Microstructure and tribological properties of MoS2+Zr composite coatings in high humidity environment. Appl. Surf. Sci., 367: 140-146.
70. Zabinski, J.S., Donley, M.S., Walck, S.D., Schneider, T.R. and McDevitt, N.T. (1995). The effects of dopants on the chemistry and tribology of sputter-deposited MoS2 films, Tribol. Trans. 36: 894–904.
71. Kong, N., Wei, B., Li, D., Zhuang, Y., Sun, G. and Wang, B. (2020). A study on the tribological property of MoS2/Ti–MoS2/Si multilayer nanocomposite coating deposited by magnetron sputtering. RSC Adv., 10: 9633-9642.
72. Scharf, T.W., Kotula, P. and Prasad, S.V. (2010). Friction and wear mechanisms in MoS2/Sb2O3/Au nanocomposite coatings. Acta Mater., 58: 4100-4109.
73. Fuadi Z. (2014). Analysis of Vibration Generated by the Rubbing of Flat Surfaces. Makara Journal of Technology, 18(3): 115-120.
74. Balaraju, J.N., Sankara Narayanan, T.S.N. and Seshadri, S.K. (2003). Electroless Ni-P Composite Coatings. J. Appl. Electrochem., 33: 807 -816.
75. Jiaqiang, G., Lei, L., Yating, W., Bin, S. and Wenbin, H. (2006). Electroless Ni–P–SiC composite coatings with superfine particles. Surf. Coat. Technol., 200(20-21): 5836-5842
76. Voevodin, A.A., O'Neill, J.P. and Zabinski, J.S. (1999). Tribological performance and tribochemistry of nanocrystalline WC/amorphous diamond-like carbon composites. Thin Solid Films, 342: 194-202.
77. Sahasrabudhe, H. and Bandyopadhyay, A. (2014). Laser processing of Fe based bulk amorphous alloy coating on zirconium. Surf. Coat. Technol., 240: 286-292.
78. Li, X. and Bhushan, B. (1999a). Micro/nanomechanical and tribological characterization of ultrathin amorphous carbon coatings. J. Mater. Res., 14: 2328-2337.
79. Malaki, M. and Varma, R. S. (2020). Mechanotribological Aspects of MXene-Reinforced Nanocomposites. Adv. Mater., 32: 2003154-74.
80. Marian, M., Song, G.C., Wang, B., Fuenzalida, V.M., Kraus, S., Merle, B., Tremmel, S., Wartzack, S., Yu, J. and Rosenkranz, A. (2020). Effective usage of 2D MXene nanosheets as solid lubricant – Influence of contact pressure and relative humidity. Appl. Surf. Sci., 531: 147311-21.
81. Yin, X., Jin, J., Chen, X., Rosenkranz, A. and Luo, J. (2019). Ultra-Wear-Resistant MXene-Based Composite Coating via in Situ Formed Nanostructured Tribofilm. ACS Appl. Mater. Interfaces, 11: 32569–32576.
82. Gao,X., Fu,Y.,Jiang,D., Wang, D., Weng,L., Yang,J., Sun, J., and Ming Hu, M. (2018). Responses of TMDs-metals composite films to atomic oxygen exposure, Journal of Alloys and Compounds, 765: 854-861.

83. Grutzmacher P.G., Suarez S., Tolosa A., Gachot C., Song G., Wang B., Presser V., Mücklich F., Anasori B., Rosenkranz A. (2022). Correction to Superior Wear-Resistance of Ti3C2Tx Multi-Layer Coatings. ACS Nano. 16(2):3433-3442.
84. Jahnig, T. and Lasagni Andres, F. (2020). Recent Progress on Wear-Resistant Materials: Designs, Properties, and Applications. Ind. Lubr. Tribol., 72: 1001-1030.
85. Zwahr, C., Helbig, R., Werner, C. and Lasagni, A. (2019). Fabrication of multifunctional titanium surfaces by producing hierarchical surface patterns using laser-based ablation methods. Sci. Rep., 9: 6721-6734.
86. Tang, W., Zhou, Y., H. Zhu and H. Yang (2013). The effect of surface texturing on reducing the friction and wear of steel under lubricated sliding contact. Appl. Surf. Sci., 273: 199-204.
87. Wakuda, M., Yamauchi, Y., Kanzaki, S. and Yasuda, Y. (2003). Effect of surface texturing on friction reduction between ceramic and steel materials under lubricated sliding contact. Wear, 254: 356-363.
88. Condea, F.F., Diazb, J.A.A., Faria da Silvac, G. and Tschiptschinc, A.P. (2019). Dependence of Wear and Mechanical Behavior of Nitrocarburized/CrN/DLC Layer on Film Thickness, Materials Research. 22(02): 1-10.
89. Ghosh, S., Choudhury, D., Roy, T., Mamat, A.B., Masjuki, H.H. and Pingguan-Murphy, B. (2015). Tribological investigation of diamond-like carbon coated micro-dimpled surface under bovine serum and osteoarthritis oriented synovial fluid. Sci. Technol. Adv. Mater., 16: 1-11.
90. Duminica, F.D., BelchiL. R., Libralesso, L., Mercier, D. (2018). Investigation of Cr(N)/DLC multilayer coatings elaborated by PVD for high wear resistance and low friction applications. Surface and Coatings Technology, 337: 396-403.
91. Kim, T.S. Park, Y.G. and Wey, M.Y. (2003). Characterization of Ti-6A1-4V alloy modified by plasma carburizing process. Mater. Sci. Eng. A, 361: 275-280.
92. Budinski, K.G. (1993). The wear resistance of diffusion treated surfaces. Wear, 162–164: 757-762.
93. Lyu, P., Chen, Y., Liu, Z., Cai, J., Zhang, C., Jin, Y., Guan, Q. and Zhao, N. (2020). Surface modification of CrFeCoNiMo high entropy alloy induced by high-current pulsed electron beam. Appl. Surf. Sci., 504(8): 1-26.
94. Garcia-Giron, A., Romano, J.M., Batal, A., Dashtbozorg, B., Dong, Solanas, E.M., Angos, U., Walker, M., Penchev, P., and Dimov, S.S. (2019). Durability and Wear Resistance of Laser-Textured Hardened Stainless-Steel Surfaces with Hydrophobic Properties. Langmuir, 35: 5353-5363.
95. Li, X., Li, B., Zhang, Q., Shi, T., J. Yu, Tang, M. and Huang, X. (2016). Fabrication of micro- and nano-scale hierarchical structures on Al surface with enhanced wettability, anti-corrosion and wear resistance. Mater. Express, 6: 10-18.
96. Wu, Y., Zhao, W., Wang, W., Zhang, Y. and Xue, Q. (2016). Novel structured anodic oxide films containing surface layers and porous sublayers showing excellent wear resistance performance. RSC Adv., 6: 94074-94084.
97. Chen Z., Wu, C. Zhou H., Zhang G., Yan, H. (2022). A high-efficiency preparation method of super wear-resistant superhydrophobic surface with hierarchical structure using wire electrical discharge machining, Surface and Coatings Technology, 444:1-12

98. Chan, C.H., Tang, S.W., Mohd, N.K., Lim, W.H., Yeong, S.K. and Idris, Z. (2018). Tribological behavior of bio-lubricant base stocks and additives. Renew. Sustain. Energy Rev., 93: 145–157.
99. Miao, J., Guo, T., Ren, J., Zhang, A., Su, B. and Meng, J. (2018). Optimization of mechanical and tribological properties of FCC CrCoNi multi-principal element alloy with Mo addition. Vacuum, 149: 324–330.
100. Zafari, A., Ghasemi, H.M. and Mahmudi, R. (2013). Effect of rare earth elements addition on the tribological behavior of AZ91D magnesium alloy at elevated temperatures. Wear, 303: 98-108.
101. Qian, J.C., Zhou, Z.F., Yan, C., Li, D.J., Li, K.Y., Descartes, S., Chromik, R., Zhang, W.J., Bello, I. and Martinu, L. (2015). Tailoring the Mechanical and Tribological Properties of Sputtered Boron Carbide Films via the B1-Cx Composition. Surf. Coat. Technol., 267: 2-7.
102. Taher, M., Mao, F., Berastegui, P., Andersson, A.M. and Jansson, U. (2018). Tribol. Int., 119: 680–687.
103. Wang, H., Gee, M., Qiu, Q., Zhang, H., Liu, X., Nie, H., Song, X. and Nie, Z. (2019). Grain Size Effect on Wear Resistance of WC-Co Cemented Carbides under Different Tribological Conditions. J. Mater. Sci. Technol., 35: 2435–2446.
104. Liu, P., Kan, Q. and Yin, H. (2019). Effect of grain size on wear resistance of nanocrystalline NiTi shape memory alloy. Mater. Lett., 241: 43-46.
105. Suarez, S., Rosenkranz, A., Gachot, C. and Mucklich, F. (2014). Enhanced tribological properties of MWCNT/Ni bulk composites – Influence of processing on friction and wear behaviour. Carbon, 66: 164-171.
106. Jones, M., Nation, B., Wellington-Johnson, J., Curry, J., Kustas, A., lu, P., Chandross, M. and Argibay, N. (2020). Evidence of inverse Hall-petch behavior and low friction and wear in high entropy alloys. Sci. Rep., 10: 10151-10159.
107. Rai, P.K., Shekhar, S. and Mondal, K. (2018). Effects of grain size gradients on the fretting wear of a specially-processed low carbon steel against AISI E52100 bearing steel. Wear, 412–413: 1-13.
108. Li, Y., Wang, S. and Wang, Q. (2017). Enhancement of tribological properties of polymer composites reinforced by functionalized graphene. Compos. B.: Eng., 120: 83-91.
109. Mohseni, H., Nandwana, P., Tsoi, A., Banerjee, R. and Scharf, T.W. (2015). In situ nitrided titanium alloys: Microstructural evolution during solidification and wear. Acta Mater., 83: 61-74.
110. Torgerson, T.B., Mantri, S.A., Banerjee R. and T.W. Scharf (2019). Room and elevated temperature sliding wear behavior and mechanisms of additively manufactured novel precipitation strengthened metallic composites. Wear, 426–427: 942-951.
111. 105. Holmberg K., Erdemir A., (2017). Influence of tribology on global energy consumption, costs and emissions. Friction, 5: 263-284.
112. Gullino A., Matteis P. and D'Aiuto, F., (2019). Review of Aluminum-To-Steel Welding Technologies for Car-Body Applications. Metals, 9: 315-340.
113. Erdemir A., Holmberg K., Coating Technology for Vehicle Applications. Eds: Cha, S.C. and Erdemir A., Springer Int. Publishing, Cham: 2015, pp. 1-248.

114. Holmberg K., Andersson P., Erdemir A., (2012). Global energy consumption due to friction in passenger cars. Tribol. Int., 47: 221-234.
115. Wang Y.M., Voisin T., McKeown J.T., Ye J., Calta N.P., Li Z., Zeng Z., Zhang Y., Chen W., Roehling T. T., Ott R. T., Santala M. K., Depond P. J., Matthews M. J., Hamza A. V., Zhu T., (2018). Additively manufactured hierarchical stainless steels with high strength and ductility. Nat. Mater., 17: 63-71.
116. Martin J.H., Yahata B.D., Hundley J.M., Mayer J.A., Schaedler T.A., Pollock T.M., (2017). 3D printing of high-strength aluminium alloys. Nature, 549: 365-369.
117. Jovicevic-Klug, P.; Podgornik, B. (2020). Review on the Effect of Deep Cryogenic Treatment of Metallic Materials in Automotive Applications, Metals, 10(4): 1-12.
118. Jovicevic-Klug, P.; Podgornik, B. (2020). Comparative study of conventional and deep cryogenic treatment of AISI M3:2 (EN 1.3395) high-speed steel. J. Mater. Res. Technol., 9: 13118–13127.
119. Jovicevic-Klug P., Jenko M., Jovicevic-Klug M., Batic B.S., Kovac, J. and Podgornik B. (2021). Effect of deep cryogenic treatment on surface chemistry and microstructure of selected high-speed steels. Applied Surface Science. 548: 1-11.
120. Senthilkumar D. (2016). Cryogenic Treatment: Shallow and Deep. First Edition; Encyclopedia of Iron, Steel, and Their Alloys, CRC Press: Pp: 1-13. ISBN 9781351254502.
121. Jovicevic-Klug P., Sedlacek M., Jovicevic-Klug M. and Podgornik B. (2021). Effect of Deep Cryogenic Treatment on Wear and Galling Properties of High-Speed Steels. Materials, 14: 1-16.
122. Ciski, A., Wach, P., Jelenkowski, J., Nawrocki, P. and Hradil, D. (2019). Deep Cryogenic Treatment and Nitriding of 42CrMo4 Steel. HTM Journal of Heat Treatment and Materials, 74 (1): 12-22.
123. Li B., Li C., Wang Y. and Jin X. (2018). Effect of Cryogenic Treatment on Microstructure and Wear Resistance of Carburized 20CrNi2MoV Steel. Metals, 8: 1-13.
124. Amini K., Akhbarizadeh A. (2012). Javadpour S. Investigating the effect of holding duration on the microstructure of 1.2080 tool steel during the deep cryogenic heat treatment. Vacuum, 86:1534–1540.
125. Paydar H.. Amini K. and Akhbarizadeh A. (2014). Investigating the effect of deep cryogenic heat treatment on the wear behavior of 100Cr6 alloy steel. Kovove Materialy-Metallic Materials, 52: 163-169.
126. Amini K., Akhbarizadeh A., Javadpour S. (2014). Investigating the effect of quench environment and deep cryogenic treatment on the wear behavior of AZ91. Mater. Des., 54: 154–160.
127. Baldissera P. (2009). Fatigue scatter reduction through deep cryogenic treatment on the 18NiCrMo5 carburized steel. Mater. Des.; 30: 3636–3642.
128. Baldissera, P.; Delprete, C. (2009). Effects of deep cryogenic treatment on static mechanical properties of 18NiCrMo5 carburized steel. Mater. Des., 30: 1435–1440
129. Firouzdor V., Nejati E. and Khomamizadeh F. (2008). Effect of deep cryogenic treatment on wear resistance and tool life of M2 HSS drill. Journal of Materials Processing Technology, 206(1): 467-472

130. Akhbarizadeh A., Javadpour S. (2013). Investigating the effect of as-quenched vacancies in the final microstructure of 1.2080 tool steel during the deep cryogenic heat treatment. Mater. Lett.,93: 247–250.
131. Jovicevic-Klug P., Sedlacek M., Jovicevic-Klug M. and Podgornik B. (2021). Effect of Deep Cryogenic Treatment on Wear and Galling Properties of High-Speed Steels. Materials, 14: 1-16.
132. Jovicevic-Klug P., Jenko M., Jovicevic-Klug M., Batic B.S., Kovac, J. and Podgornik B. (2021). Effect of deep cryogenic treatment on surface chemistry and microstructure of selected high-speed steels. Applied Surface Science. 548: 1-11.
133. Jovicevic-Klug M., Jovicevic-Klug P., Kranjec T., Podgornik B. (2021). Cross-effect of surface finishing and deep cryogenic treatment on corrosion resistance of AISI M35 steel. Journal of Materials Research and Technology, 14: 2365-2381.
134. Xu, G.; Huang, P.; Wei, Z.; Feng, Z.; Zu, G. (2022). Microstructural variations and mechanical properties of deep cryogenic treated AISI M35 high-speed steel tempered at various temperatures. J. Mater. Res. Technol.,17, 3371–3383.
135. Fantineli D.G., Parcianello C.T., Rosendo T.S., Reguly A. and Tier M.D. (2020). Effect of heat and cryogenic treatment on wear and toughness of HSS AISI M2. J. of Mat. Res. and Tech., 9: 12354-12363.
136. Zhou L., Min N., Li H., Wu X. (2019). Nanoscratch and internal friction investigations of deep cryogenic treated M2 high-speed steel. Heat Treatment and Surface Engineering, 1 (3-4): 1-7.
137. Zhang H., Sun M., Liu Y., Ma D., Xu B., Huang M., Li D. and Li Y. (2021). Ultrafine-grained dual-phase maraging steel with high strength and excellent cryogenic toughness. Acta Materialia, 211: 1-14.
138. Bi J, Li L., Peng J., Liao J. and Yuan Gao Y. (2021). Effect of deep cryogenic treatment on microstructure and properties of M35 high speed steel., 2044(1):012014 :1-9.
139. Sreerama Reddy T.V., Sorna T.K., Venkatarama M.R., Ajaykumar, B.S. (2008). Performance studies of deep cryogenic treated tungsten carbide cutting tool inserts on machining steel. Tribology - Materials Surfaces & Interfaces, 2(2): 92-98.
140. Vadivel K., Rudramoorthy R. (2009). Performance analysis of cryogenically treated coated carbide inserts. Int J Adv Manuf Technol, 42: 222-232.
141. Jovicevic-Klug P., Jovicevic-Klug M. and Podgornik B. (2021). Unravelling the Role of Nitrogen in Surface Chemistry and Oxidation Evolution of Deep Cryogenic Treated High-Alloyed Ferrous Alloy. Coatings 2022, 12: 1-15.
142. Kang C., Liu F., Jiang Z., Suo H., Yu X., Zhang H. and Ding S. (2021). Effect of cryogenic treatment on microstructure evolution and mechanical properties of high nitrogen plastic die steel. Journal of Materials Research and Technology, 15: 5128-5140.
143. Amini K., Akhbarizadeh A., Javadpour S. (2014). Investigating the effect of quench environment and deep cryogenic treatment on the wear behavior of AZ91. Mater. Des., 54: 154–160.
144. Yong J., Ding C. and Qiong (2012). Effect of cryogenic thermocycling treatment on the structure and properties of magnesium alloy AZ91. Metal Science and Heat Treatment, 53(11-12). 18-21.

145. Jovicevic-Klug P., Pus G, Jovicevic-Klug M., Zuzek B, Podgornik B. (2022). Influence of heat treatment parameters on effectiveness of deep cryogenic treatment on properties of high-speed steels. Materials Science and Engineering: A., 829: 1-12.
146. Gu K., Wang J. and Zhou Y. (2014). Effect of cryogenic treatment on wear resistance of Ti–6Al–4V alloy for biomedical applications. Journal of the Mechanical Behavior of Biomedical Materials, 30: 131-139.
147. Li B., Li C., Wang Y. and Jin X. (2018). Effect of Cryogenic Treatment on Microstructure and Wear Resistance of Carburized 20CrNi2MoV Steel., Metals, 8: 1-13.
148. Siddaiah A., Mao B., Liao Y. and Menezes P. (2018). Surface characterization and tribological performance of laser shock peened steel surfaces. Surface and Coatings Technology, 351: 188-197.
149. Nazir, M.H., Khan Z.A., Saeed A. and Siddaiah A. (2018). Synergistic Wear-Corrosion Analysis and Modelling of Nanocomposite Coatings., 121: 1-15.
150. Cho S., Ko S.J., Yoo J.S., Park J.C., Yoo Y.H. and Kim J.G. (2021). Optimization of pickling solution for improving the phosphatability of advanced high-strength steels. Materials, 14(1): 1-15.
151. Wang W., Du M., Zhang X., Luan C. and Tian Y. (2021). Preparation and Properties of Mo Coating on H13 Steel by Electro Spark Deposition Process. Materials, 14(13): 1-16.
152. Parchovianska I., Parchovianska M., Kankova h., Nowicka A. and Galusek D. (2021). Hydrothermal corrosion of double layer glass/cramic coatings obtained from preceramic polymers. Materials, 14: 1-18.
153. Parchovianska M., Parchovianska I., Svancarek P., Medved D., Lenz-Leite M., Motz G. and Galusek D. (2021). High-temperature oxidation resistance of PDC coatings in synthetic Air and water vapor atmospheres. Molecules, 26: 1-17.
154. Shen Y., Luo J., Liao B., Chen L., Zhang X., Zhao Y. and Pang P. (2022). Enhanced Anti-Tribocorrosion Performance of Ti-DLC Coatings Deposited by Filtered Cathodic Vacuum Arc with theOptimization of Bias Voltage. Coatings, 12: 1-14.
155. Siddaiah A., Mao B., Liao Y. and Menezes P. (2018). Surface characterization and tribological performance of laser shock peened steel surfaces. Surface and Coatings Technology, 351: 188-197.
156. Nazir MH, Khan ZA, Saeed A, Siddaiah A, Menezes PL. Synergistic wear-corrosion analysis and modelling of nanocomposite coatings. Tribology International. 2018; 121:30-44.
157. Siddaiah A., Mao B., Liao Y., Menezes P. (2019). Effect of laser shock peening on the wear–corrosion synergistic behavior of an az31b magnesium alloy. Journal of Tribology 142(4): 1-22.
158. Wang H, Huang Y, Zhang W, Ostendorf A. (2018). Investigation of multiple laser shock peening on the mechanical property and corrosion resistance of shipbuilding 5083Al alloy under a simulated seawater environment. Appl Opt., 57:6300-6308.
159. Jokari M., Mahboubi F. and Dehghani K. (2017). Structure and tribological behavior of diamond-like carbon coatings deposited on the martensitic stainless steel: The influence of gas composition and temperature. Diamond and Related Materials, 77: 1-12.

160. Mohamed M.E. and Abd-El-Nabey B.A. (2022). Corrosion performance of a steel surface modified by a robust graphene-based superhydrophobic film with hierarchical roughness. Journal of Materials Science, 57: 11376–11391.

Appendixes: Schematic of wear test system (see reference in Table 2)

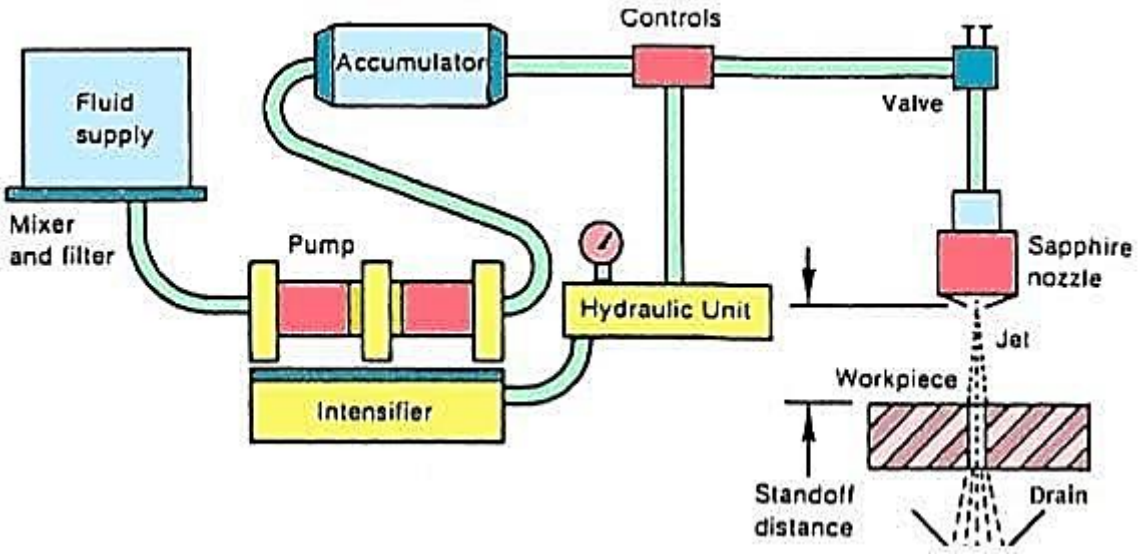

Appendix A. Fluid jet system , ASTM A532-ClassIII A

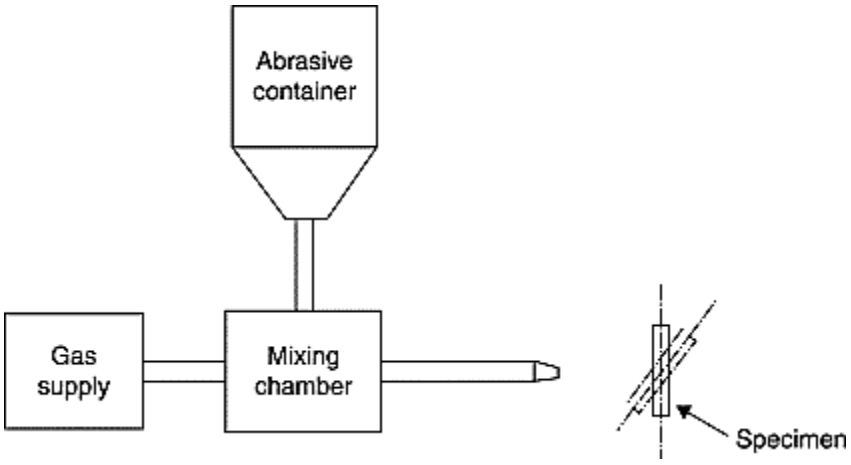

Appendix B. Gas blast erosion test system, ASTM G76

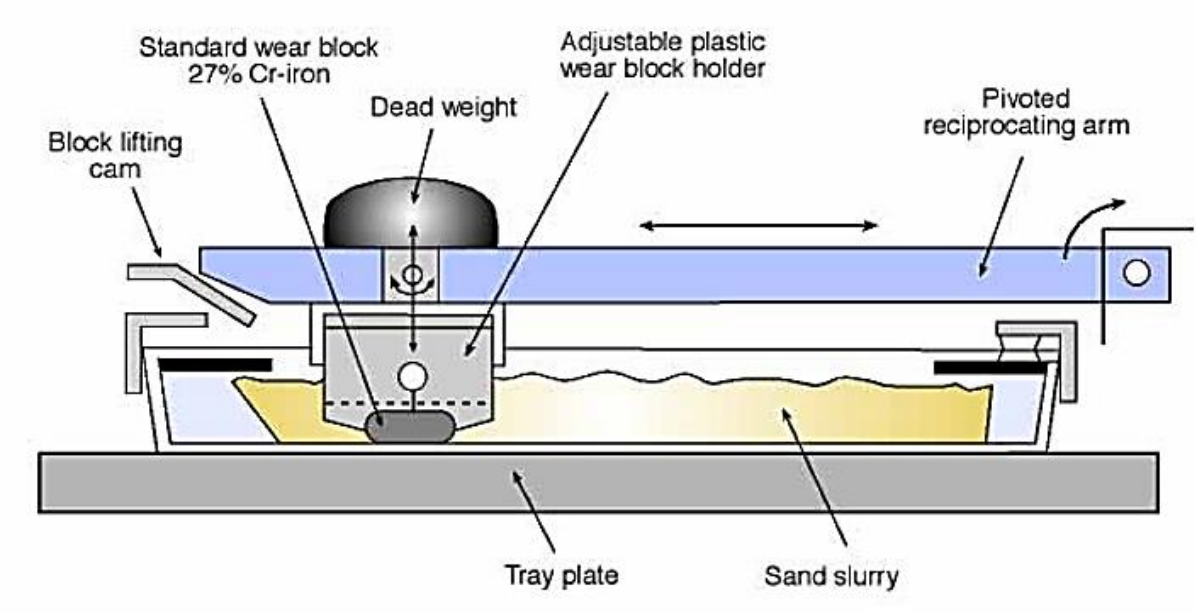

Appendix C. Loose slurry abrasive testing ASTM G65

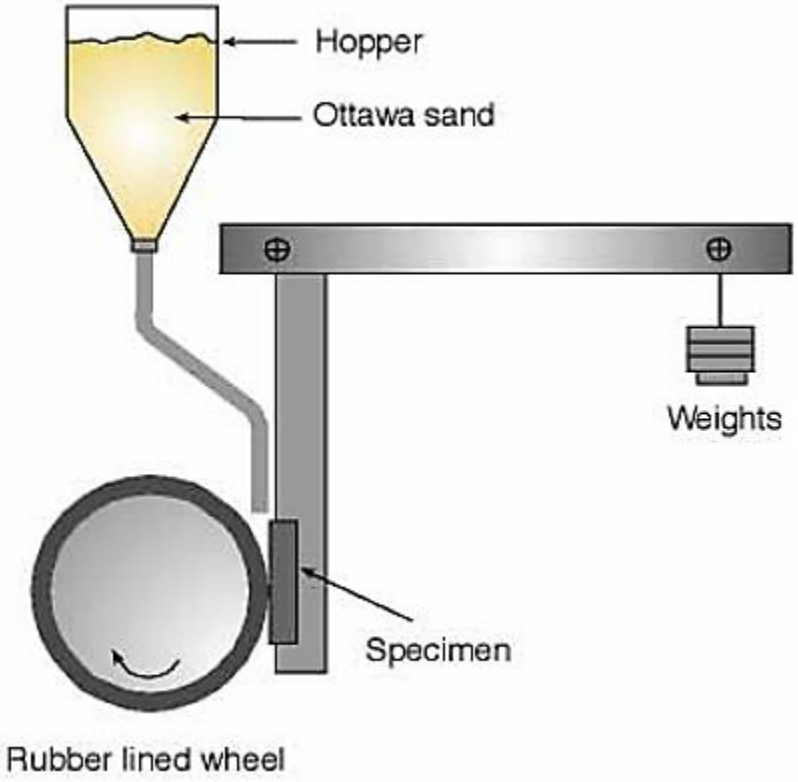

Appendix D. Rubber wheel, dry abrasive, ASTM G65

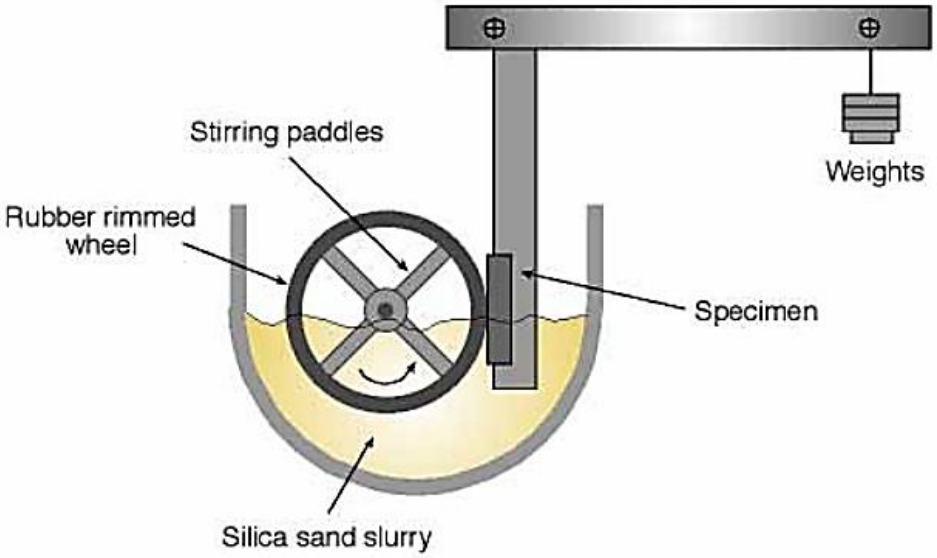

Appendix E. Rubber wheel, wet abrasive slurry, ASTM 105

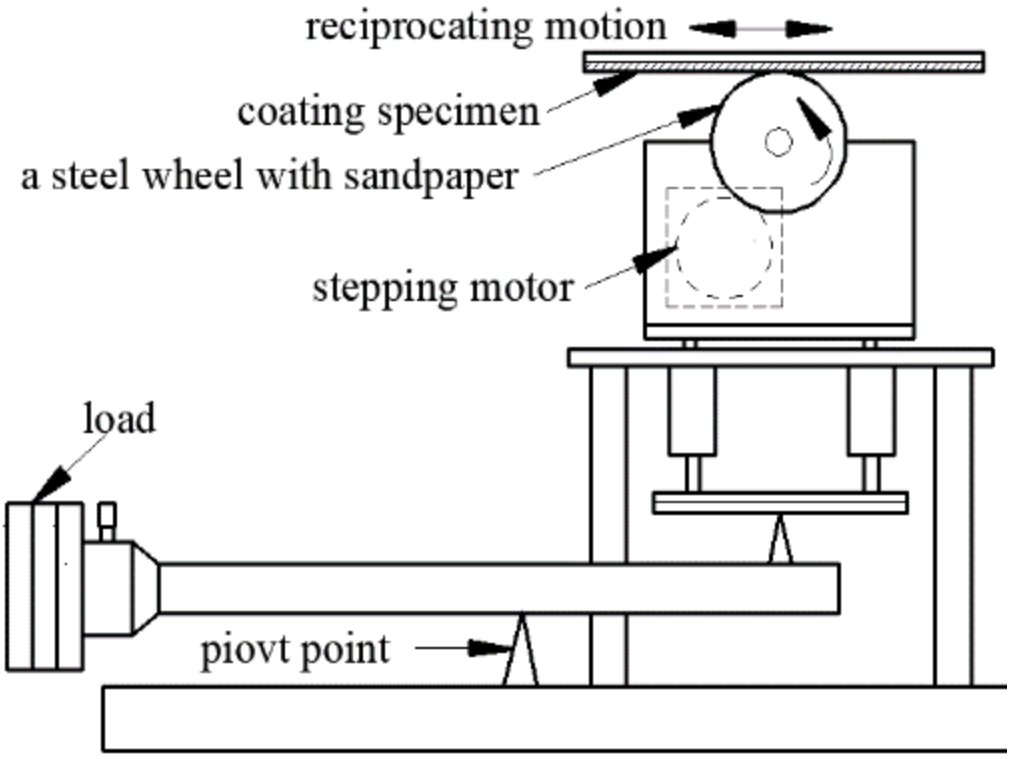

Appendix F. The two-body abrasive wear test apparatus., ASTM B611

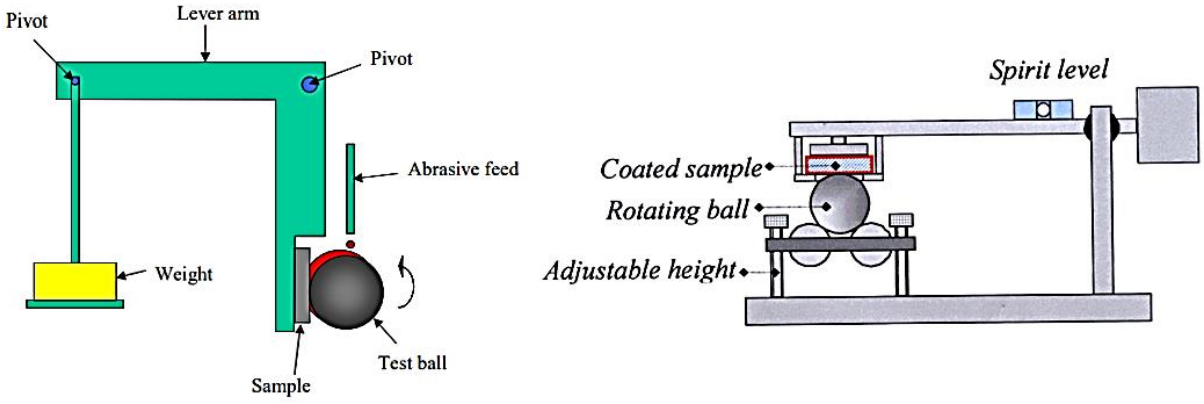

Appendix G. Ball Cratering Equipment (two-types)

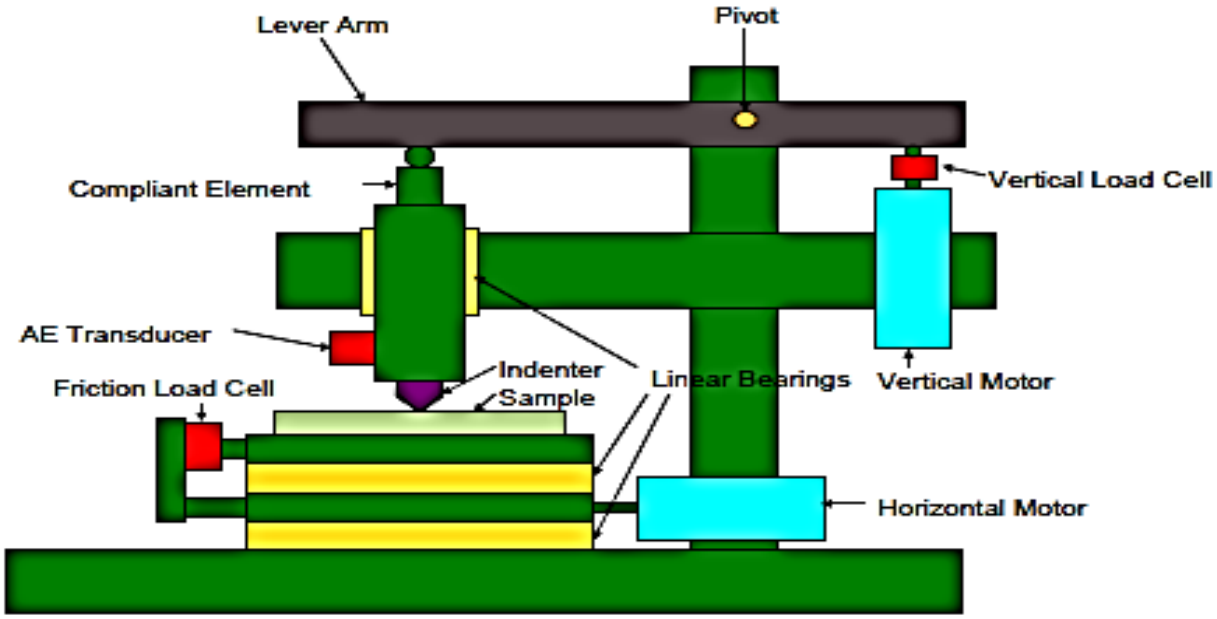

Appendix E. Scratch testing system

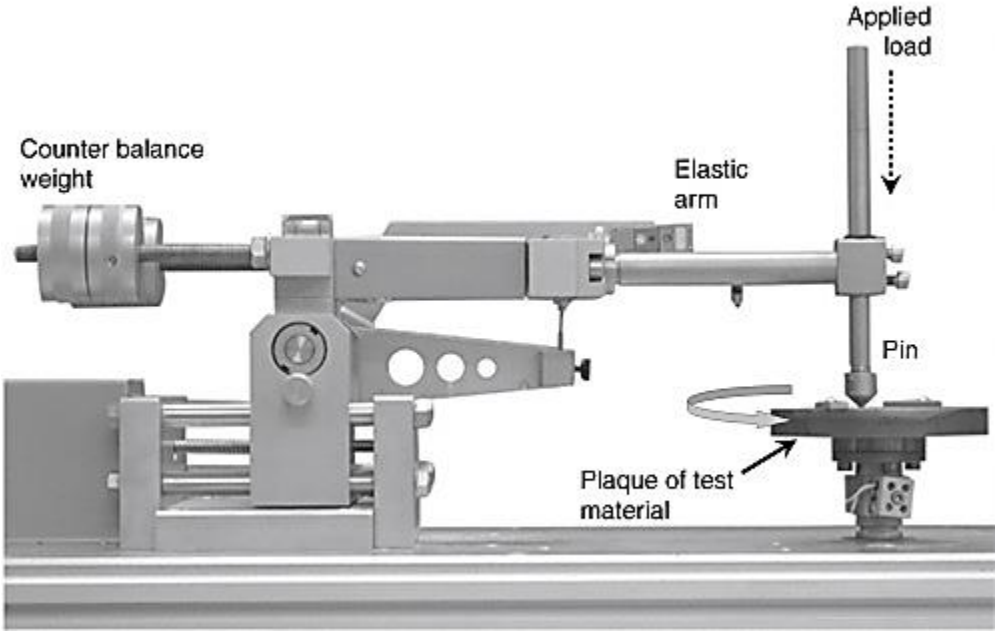

Appendix I. Pin-on-disc system

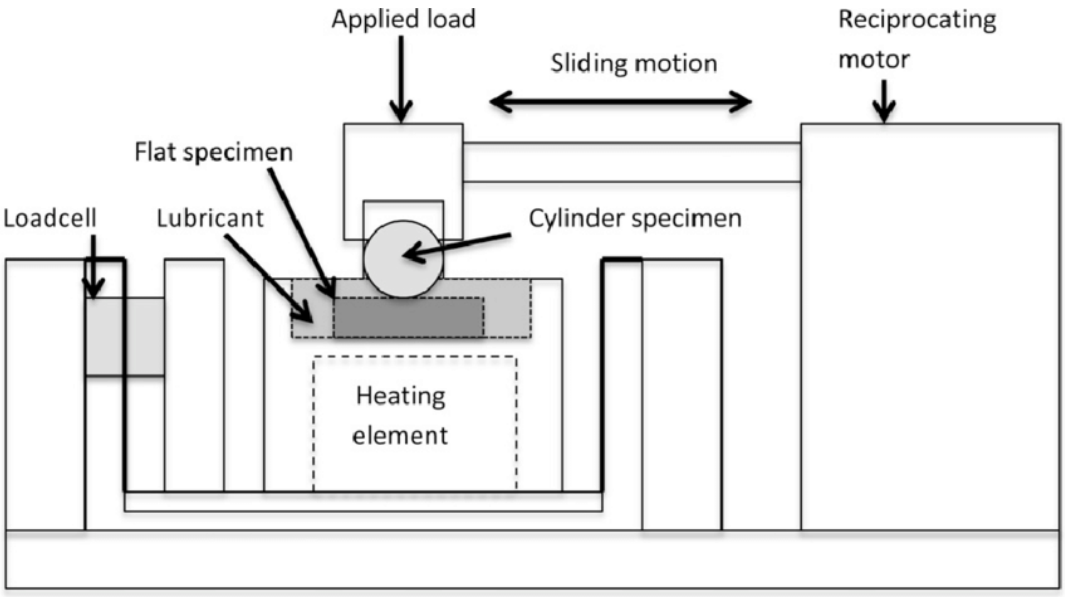

Appendix J. Reciprocating test system (ASTM G133)

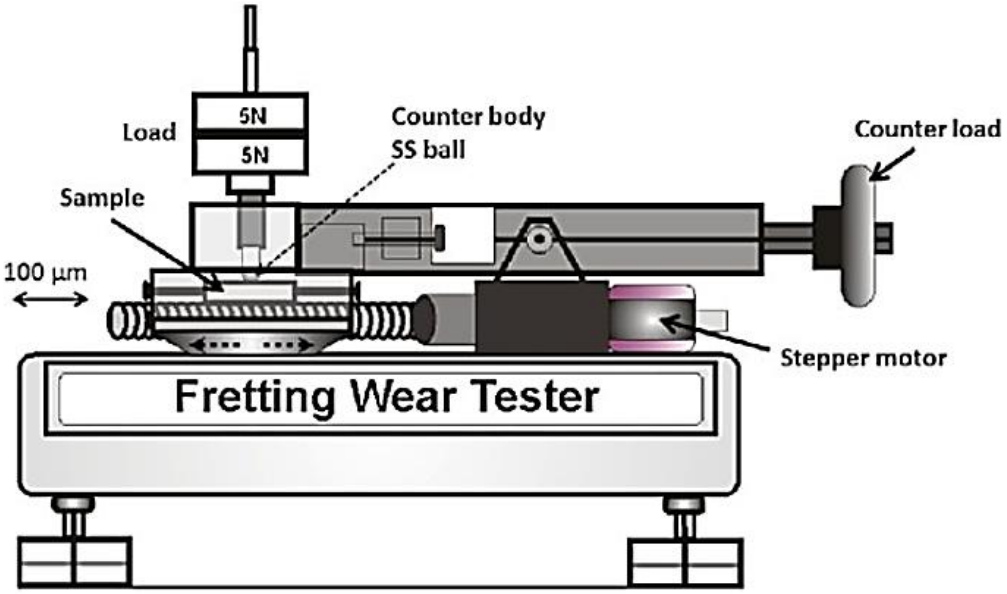

Appendix K. Fretting wear tester

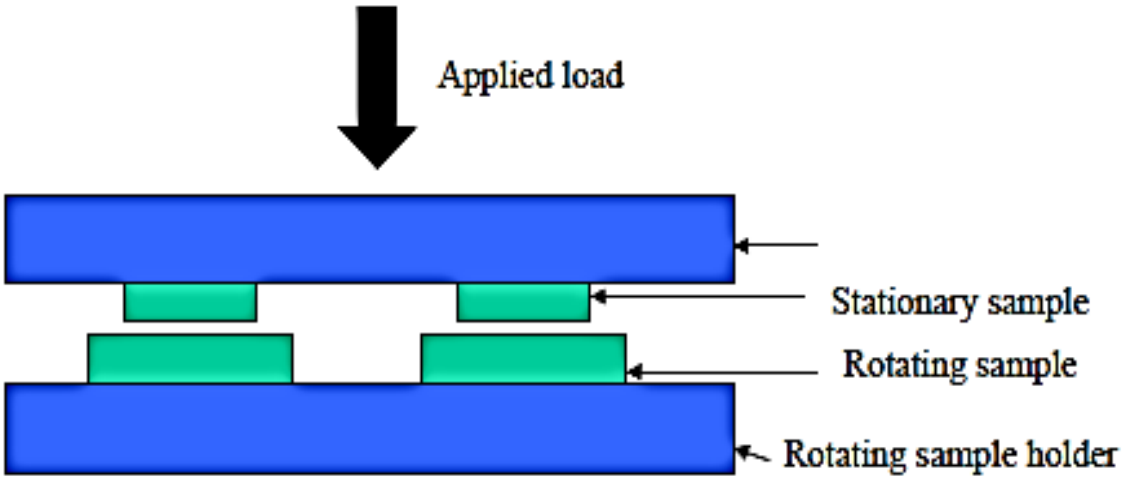

Appendix L. Thrust washer test arrangement for Sliding wear

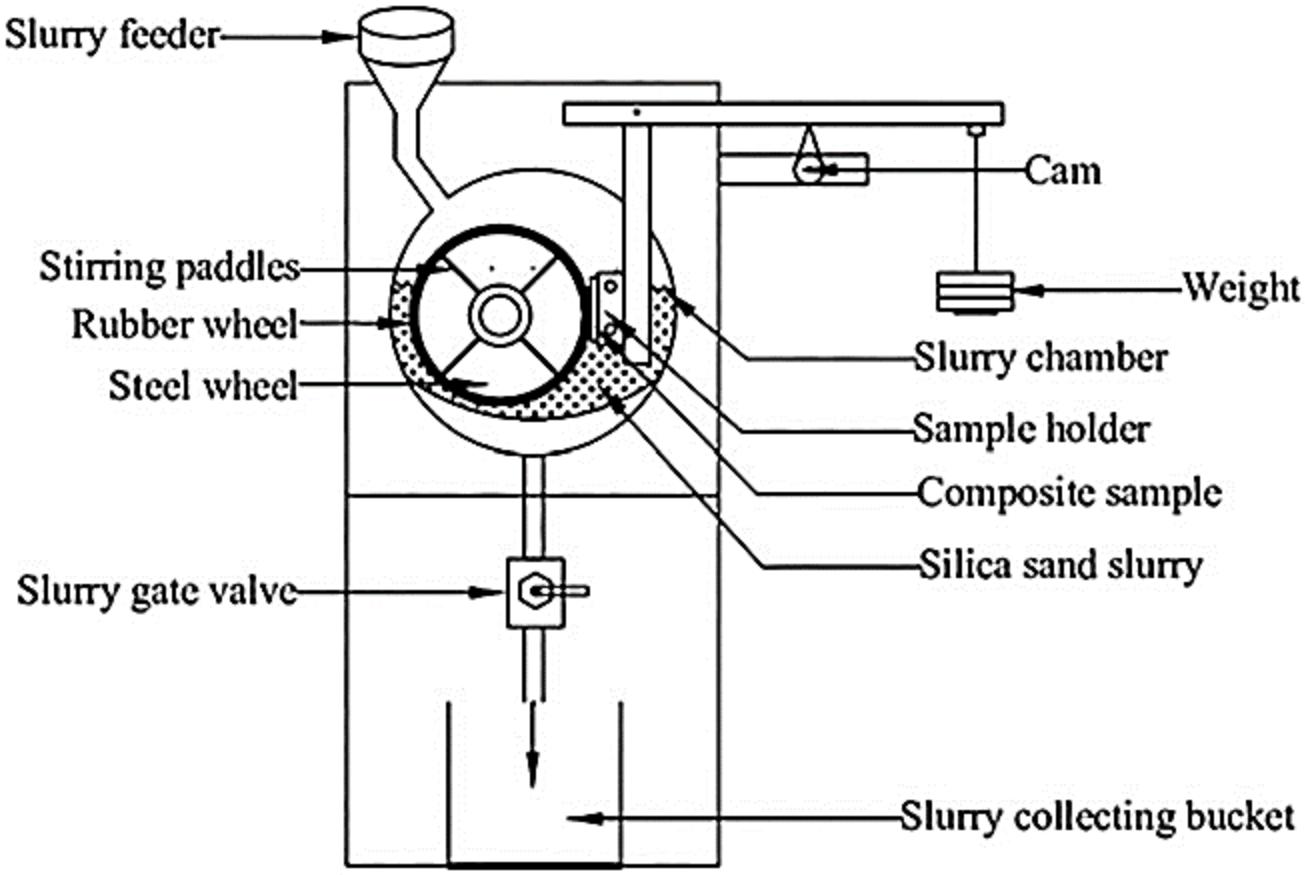

Appendix M. Schematic of the set-up of Slurry erosion test

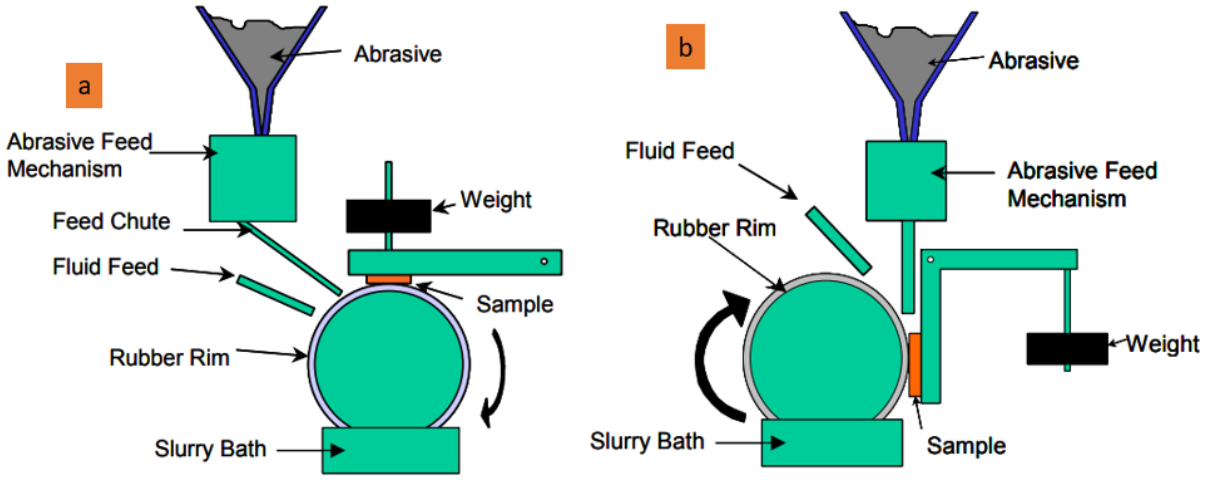

Appendix O. Rotating Abrassive wear test (a) horizontal workpiece (b) vertical workpiece